MEASUREMENT OF THE DEUTERON MAGNETIC FORM FACTOR AT LARGE MOMENTUM TRANSFERS

Jefferson Lab PAC24 Proposal
April 2003

R. Alarcon
Arizona State University, Tempe, AZ 85287

K.A. Aniol, D.J. Margaziotis
California State University, Los Angeles, CA 90032

L. Todor
Carnegie Mellon University, Pittsburgh, PA 15213

W. Boeglin, P.E.C. Markowitz
Florida International University, Miami, FL 33199

R. De Leo, L. Lagamba
INFN/Bari and University of Bari, 70126 Bari, Italy

F. Cusanno, S. Frullani, F. Garibaldi, M. Iodice, G.M. Urciuoli
INFN/Sanità and ISS Physics Lab., 00161 Rome, Italy

J. Gomez, F. Gross, D.W. Higinbotham, C.W. de Jager, S.K. Nanda, A. Saha
Jefferson Lab, Newport News, VA 23606

A. Adeluyi, B.D. Anderson, A.T. Katramatou, D.M. Manley, G.G. Petratos, J.W. Watson
Kent State University, Kent, OH 44242

W. Korsch
University of Kentucky, Lexington, KY 40506

E.J. Beise, H. Breuer, C.-C. Chang, J.J. Kelly, P. King, P. Roos
University of Maryland, College Park, MD 20742

R.S. Hicks, K.S. Kumar, R.A. Miskimen, G.A. Peterson
University of Massachusetts, Amherst, MA 01003

W. Bertozzi, O. Gayou, S. Gilad, P. Monaghan, R. Suleiman
Massachusetts Institute of Technology, Cambridge, MA 02139

J.R. Calarco
University of New Hampshire, Durham, NH 03824

J.A. Templon
NIKHEF, 1009 DB Amsterdam, The Netherlands

P.E. Ulmer, J.W. Van Orden
Old Dominion University, Norfolk, VA 23529

L. Bimbot
Institut de Physique Nucléaire, F-91406 Orsay, France

R. Gilman, K. McCormick, R.D. Ransome, X. Jiang
Rutgers, The State University of New Jersey, Piscataway, NJ 08855

A.J. Sarty
Saint Mary's University, Halifax, NS B3H3C3, Canada

P. Decowski
Smith College, Northampton, MA 01063

E. Piasetzky
Tel Aviv University, Tel Aviv 69978, Israel

F. Butaru, S. Choi, Z.-E. Meziani, Y. Yao
Temple University, Philadelphia, PA 19122

Y. Fujii, O. Hashimoto, S. Nakamura
Tohoku University, Sendai 980-77, Japan

Spokesperson: G.G. Petratos

Co-spokespersons: E.J. Beise and J. Gomez

Abstract

We repropose an experiment on a precision measurement of the deuteron $B(Q^2)$ magnetic form factor over its diffraction minimum and possibly up to $Q^2 = 6$ (GeV/c)^2, limited only by cross section sensitivity. The experiment can be performed in the JLab Hall A Facility using a 180° custom-made spectrometer to detect back-scattered electrons and a 0° spectrometer based on the hadron HRS to detect forward-recoiling deuterons in coincidence. The experiment will also be able to measure elastic electron-proton scattering up to $Q^2 = 10.5$ (GeV/c)^2 and provide data on the proton G_M^p magnetic form factor, free of Rosenbluth separation experimental deficiencies. The deuteron results are expected to play a crucial role in understanding the internal structure and dynamics of the deuteron. The new $B(Q^2)$ data will offer unique grounds for testing non-relativistic and relativistic models of the nucleon-nucleon interaction and meson-exchange currents, as well as ideas based on quark degrees of freedom and perturbative QCD. The precision of the $B(Q^2)$ data will constrain the theoretical uncertainties and hopefully result in a consistent canonical hadronic model describing the electromagnetic structure of the simplest nucleus in nature. The new G_M^p data will be highly complementary to recent precise JLab polarization data on the proton G_E^p electric form factor and will provide valuable input in understanding the extraction of the proton elastic form factors from polarized and unpolarized measurements. We request the resources to design, build and commission the 180°/0° magnetic spectrometer and associated beam transport system, and a liquid deuterium/hydrogen target system with short scattering chamber diameter. The experiment requires beam energies in the range of 0.7 to 6.0 GeV, beam currents of 150 μA, 50 days of deuterium and hydrogen data taking at 100% efficiency, and a minimum of 15 days of check-out time.

1 Theory Overview

Electron scattering from the deuteron has long been a crucial tool in understanding the internal structure and dynamics of the nuclear two-body system [1, 2, 3, 4]. In particular, the deuteron electromagnetic form factors, measured in elastic scattering, offer unique opportunities to test models of the short-range nucleon-nucleon interaction and meson-exchange currents as well as the possible influence of explicit quark degrees of freedom [5].

The cross section for elastic electron-deuteron scattering is described, in the one-photon exchange approximation, by the Rosenbluth formula:

$$\frac{d\sigma}{d\Omega} = \frac{\alpha^2 E'}{4E^3 \sin^4\left(\frac{\theta}{2}\right)} \left[A(Q^2)\cos^2\left(\frac{\theta}{2}\right) + B(Q^2)\sin^2\left(\frac{\theta}{2}\right) \right], \tag{1}$$

where E and E' are the incident and scattered electron energies, θ is the electron scattering angle, $Q^2 = 4EE'\sin^2(\theta/2)$ is the four-momentum transfer squared and α is the fine-structure constant. The elastic structure functions $A(Q^2)$ and $B(Q^2)$ are given in terms of the charge, quadrupole and magnetic form factors of the deuteron $G_C(Q^2)$, $G_Q(Q^2)$ and $G_M(Q^2)$:

$$A(Q^2) = G_C^2(Q^2) + \frac{8}{9}\tau^2 G_Q^2(Q^2) + \frac{2}{3}\tau G_M^2(Q^2), \tag{2}$$

$$B(Q^2) = \frac{4}{3}\tau(1+\tau)G_M^2(Q^2), \tag{3}$$

where $\tau = Q^2/4M_d^2$, with M_d being the deuteron mass. Since $A(Q^2)$ is dominated by the two electric form factors and since $B(Q^2)$ is directly proportional to the magnetic one, it is customary to call $A(Q^2)$ and $B(Q^2)$ the electric and magnetic deuteron form factors, respectively. This convention will be followed throughout the text.

Separation of the two $A(Q^2)$ and $B(Q^2)$ elastic structure functions is accomplished by cross section measurements at different scattering angles. Forward angle scattering [6] yields $A(Q^2)$, while backward angle scattering [7] allows for the determination of $B(Q^2)$. Separation of all three $G_C(Q^2)$, $G_Q(Q^2)$ and $G_M(Q^2)$ form factors is achieved by measuring a polarization observable in a single- or double-scattering experiment [8, 9]. Single-scattering experiments have used unpolarized electron beams and tensor-polarized deuteron targets [10]. Double-scattering experiments have used unpolarized electron beams and recoil deuteron tensor polarimeters [11].

Cross section asymmetry measurements with an electron beam and a tensor-polarized target or a deuteron tensor polarimeter, result in the extraction of the deuteron tensor polarization observable $t_{20}(Q^2)$, which is given in terms of the deuteron form factors as:

$$t_{20}(Q^2) = -\frac{1}{\sqrt{2}S(Q^2)}\left[\frac{8}{3}\tau G_C(Q^2)G_Q(Q^2) + \frac{8}{9}\tau^2 G_Q^2(Q^2) + \frac{1}{3}\tau f(\theta)G_M^2(Q^2)\right], \tag{4}$$

where $S(Q^2) = A(Q^2)+B(Q^2)\tan^2(\theta/2)$ and $f(\theta) = 1+2(1+\tau)\tan^2(\theta/2)$. It is customary to neglect the small contribution of $G_M(Q^2)$ in $t_{20}(Q^2)$ and use the alternate quantity $\tilde{t}_{20}(Q^2)$, defined as:

$$\tilde{t}_{20}(Q^2) = \sqrt{2}\frac{y(2+y)}{1+2y^2}, \qquad y = \frac{2\tau G_Q(Q^2)}{3G_C(Q^2)}. \tag{5}$$

The advantage of this quantity is that, in both the non-relativistic and relativistic impulse approximation, it is independent of the nucleon electromagnetic form factors, as they cancel in the ratio $G_Q(Q^2)/G_C(Q^2)$.

In the non-relativistic impulse approximation (IA), the electron interacts, through the exchange of a virtual photon, with one of the two moving nucleons in the deuteron (see Figure 1a), and the two-body bound state is solved using the Schrödinger equation with a realistic nucleon-nucleon potential. The deuteron form factors are then described in terms of the deuteron wave function and the electromagnetic form factors of the nucleons [12]:

$$G_C = (G_E^p + G_E^n)C_E, \tag{6}$$

$$G_Q = (G_E^p + G_E^n)C_Q, \tag{7}$$

$$G_M = \frac{M_d}{M}\left[(G_M^p + G_M^n)C_S + \frac{1}{2}(G_E^p + G_E^n)C_L\right], \tag{8}$$

where G_E^p and G_M^p are the electric and magnetic form factors of the proton, G_E^n and G_M^n are the electric and magnetic form factors of the neutron, and M is the nucleon mass. The factors C_E, C_Q, C_S and C_L give the distribution of the proton and neutron point currents inside the deuteron as determined by the deuteron wave function. They are integrals of quadratic combinations of the S- and D-state wave functions $u(r)$ and $w(r)$ of the deuteron, with r being the internucleon separation, expressed as:

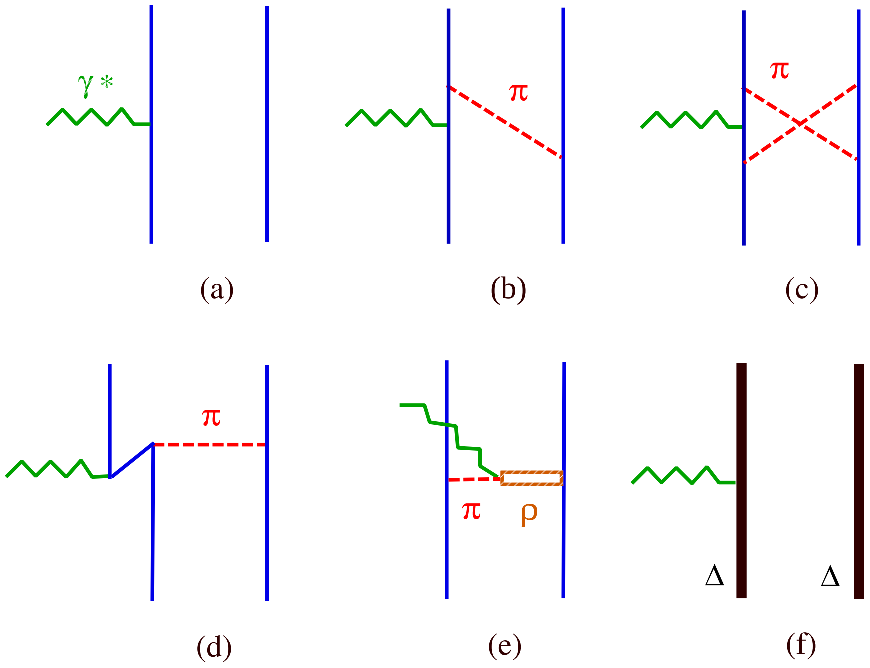

Figure 1: Non-relativistic diagrammatic representation of elastic electron-deuteron scattering. (a): impulse approximation; (b-e): selected meson-exchange current diagrams (retardation correction, two-pion exchange current, pair current and $\rho\pi\gamma$ interaction current) ; (f): isobar configuration.

$$C_E = \int_0^\infty \left[u^2(r) + w^2(r)\right] j_0(k) dr, \tag{9}$$

$$C_Q = \frac{3}{\sqrt{2}\tau} \int_0^\infty w(r) \left[u(r) - \frac{w(r)}{2\sqrt{2}}\right] j_2(k) dr, \tag{10}$$

$$C_S = \int_0^\infty \left[u^2(r) - \frac{w^2(r)}{2}\right] j_0(k) + \frac{w(r)}{2}\left[\sqrt{2}u(r) + w(r)\right] j_2(k) dr, \tag{11}$$

$$C_L = \frac{3}{2} \int_0^\infty w^2(r) \left[j_0(k) + j_2(k)\right] dr, \tag{12}$$

where $j_0(k)$ and $j_2(k)$ are spherical Bessel functions, with $k = Qr/2$.

Theoretical calculations based on the IA approach using various nucleon-nucleon potentials and parametrizations of the nucleon form factors underestimate the $A(Q^2)$ data and fail to reproduce the position of the first diffraction minimum and the height of the secondary maximum of the charge and magnetic form factor data (for extended theory and experiment reviews, and compilations of experimental data see References [1], [2], [3], [4] and [13]). It has long been known that the deuteron form factors are very sensitive to the presence of meson-exchange currents (MEC) and/or relativistic effects in the deuteron. The inclusion of "model independent" (Figure 1b, 1c, 1d) and "model dependent" (Figure 1e) MEC to the IA brings the theory into better agreement with the data but still fails to describe at the same time all available deuteron form factor data for moderate and large momentum transfer measurements [2, 3]. It should be noted that some calculations of the deuteron form factors show also sensitivity to possible presence of isobar configurations (Figure 1f) in the deuteron wave function [14, 15], but the magnitude of these configurations is essentially unknown. In general, inclusion of reasonable isobar configurations in the IA does not bring the non-relativistic calculations in agreement with all available deuteron form factor data.

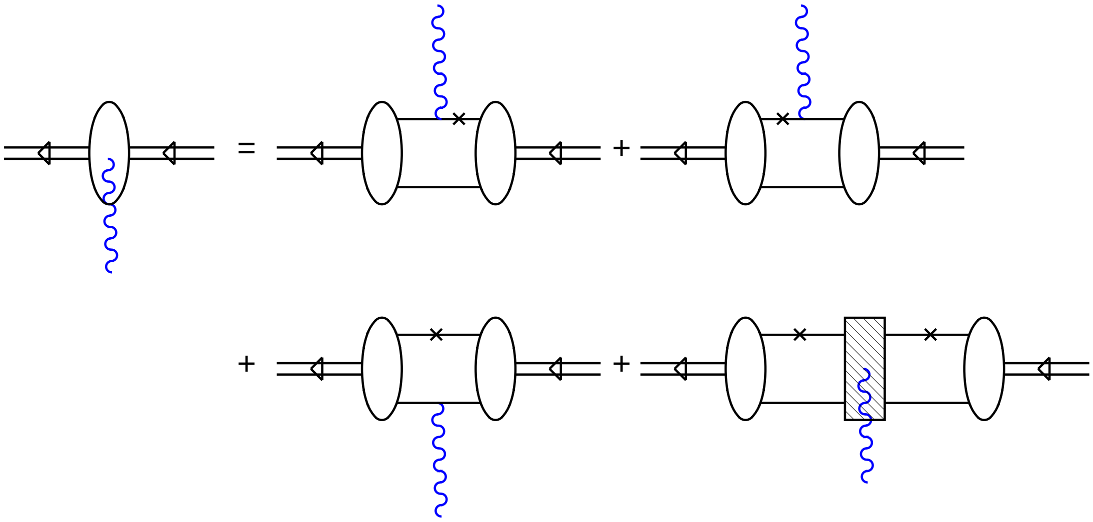

Figure 2: Feynman diagrams representing elastic electron-deuteron scattering in the Complete Impulse Approximation relativistic approach of Gross and collaborators [20]. The crosses on the nucleon lines denote on-shell particles. The shaded box depicts the $\rho\pi\gamma$ interaction current.

The failure of the non-relativistic calculations with increasing momentum transfers dictates the need for relativistic calculations. There are two relativistic approaches: Hamiltonian Dynamics [16, 17] and Propagator Dynamics [18]. In the first approach, the basic dynamics contains a finite number of particles and has a corresponding Hilbert space when quantized. The quantization is performed along constant time surfaces (instant-form dynamics), along spacelike surfaces with constant interval (point-form dynamics), or along the light cone (light-front dynamics). The advantage of the hamiltonian dynamics framework is that it can lead to equations of motion of the same form as the two-body Schrödinger equation, where it is possible to use non-relativistic nucleon-nucleon potentials without modification. The disadvantage of this formalism is, in general, the loss of locality and manifest covariance. Also, no consensus has been reached concerning consistent techniques for the construction of electromagnetic currents in this framework [2, 3].

The second approach is based on a field theory description of two interacting nucleons using three-dimensional reductions of the Bethe-Salpeter (BS) equation [19], which is a four-dimensional integral equation with a complicated analytical structure. The three-dimensional reduction to so called quasipotential equations is accomplished by replacing the free propagator in the BS equation with a new one chosen to include a constraint in the form of a delta function involving either the relative energy [20, 21] or time [22] of the interacting nucleons. The advantage of the propagator dynamics is the retainment of locality and manifest covariance. The disadvantage of this approach is the inclusion of negative energy states in the particle propagators, which tends to make the calculations technically more difficult and their physical interpretation harder. A diagrammatic representation of one of the propagator dynamics approaches by Gross and collaborators [20] is shown in Figure 2. The Figure includes also the $\rho\pi\gamma$ interaction current (shaded box). Recent dramatic advances [23, 24] in the refinement of the propagation dynamics approach have brought the theory in reasonable agreement with the experimental data (see below).

It is widely recognized that at distances much less than the nucleon size, the underlying quark-gluon dynamics of the deuteron cannot be ignored. This has led to the formulation of so called hybrid quark models [25, 26, 27], which try to simultaneously incorporate the quark- and gluon-exchange mechanism at short distances and the meson-exchange mechanism at long and intermediate distances. A commonly used approach divides the deuteron in two regions: an exterior one described by baryon configurations and an interior one described by a quark cluster. When the internucleon separation becomes smaller than $\sim$1 fm, the deuteron is treated as a six-quark configuration with a certain probability. Hybrid models are still in a phenomenological stage but the hope is that they could provide a consistent basis of bridging the meson-nucleon and quark-gluon descriptions of the few-body systems.

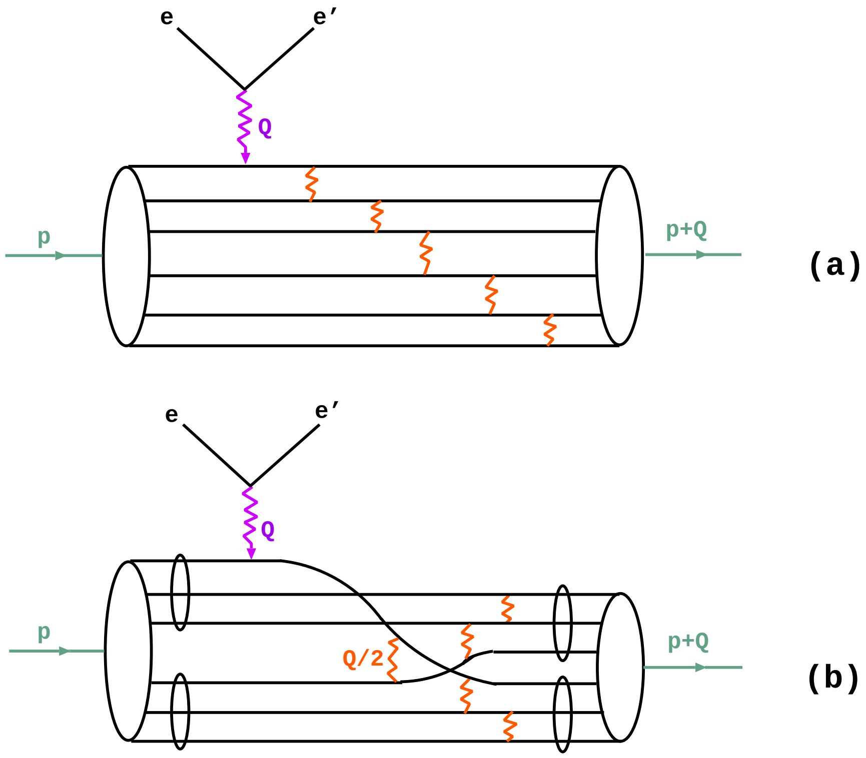

Figure 3: Elastic electron-deuteron scattering in the quark-dimensional scaling model [28, 29] showing the rescattering of the six deuteron constituent quarks (solid lines) via the exchange of hard gluons (wavy lines); (a): democratic six-quark chain model, (b) quark-interchange model.

At sufficiently large momentum transfers the deuteron form factors are expected to be calculable in terms of only quarks and gluons within the framework of Quantum Chromodynamics (QCD). The first attempt at a quark-gluon description of the deuteron form factors was based on quark-dimensional scaling (QDS) [28, 29]: the underlying dynamical mechanism during elastic electron-deuteron scattering is the rescattering of the constituent quarks via the exchange of hard gluons, which implies that $\sqrt{A(Q^2)} \sim (Q^2)^{-5}$. This prediction was later substantiated in the framework of perturbative QCD (pQCD), where it was shown [30] that to leading-order:

$$\sqrt{A(Q^2)} = \left[\frac{\alpha_s(Q^2)}{Q^2}\right]^5 \sum_{m,n} d_{mn} \left[\ln \frac{Q^2}{\Lambda^2_{QCD}}\right]^{-\gamma_n-\gamma_m}, \qquad (13)$$

where $\alpha_s(Q^2)$ and Λ_{QCD} are the QCD strong coupling constant and scale parameter, and $\gamma_{m,n}$ and d_{mn} are QCD anomalous dimensions and constants.

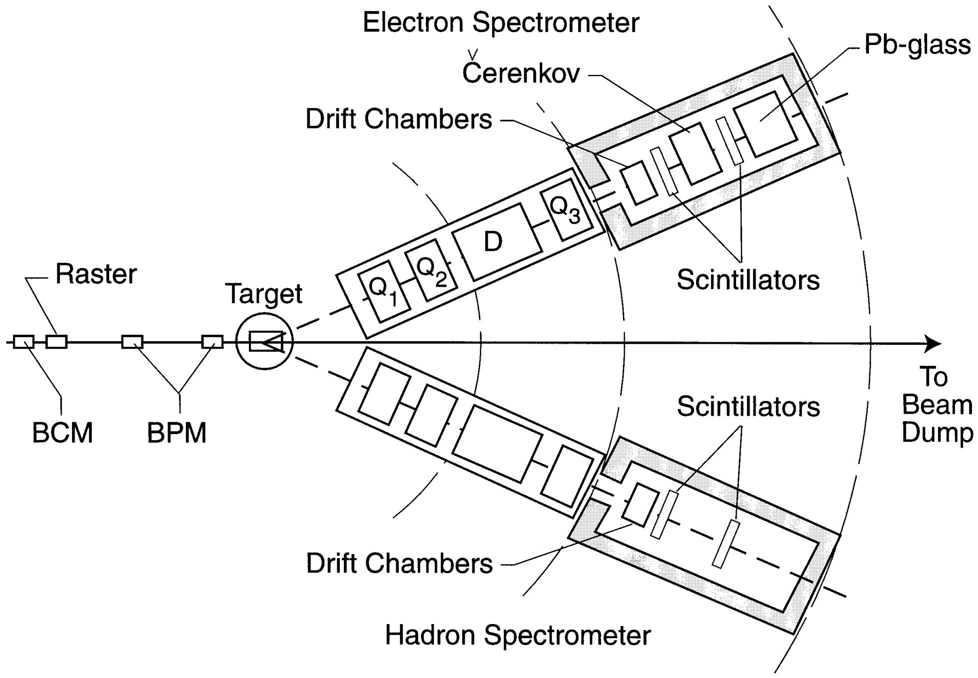

Figure 4: Plan view of the JLab Hall A Facility as used for the recent measurement of the deuteron $A(Q^2)$ at large momentum transfers [6]. Shown are the target scattering chamber, and the two identical high resolution spectrometers with their detectors, each consisting of three quadrupole Q_1, Q_2, Q_3 magnets and a dipole D magnet.

A trend consistent with the QDS and pQCD predictions for the deuteron electric form factor has been observed in recent Jefferson Lab (JLab) measurements [6]. Extension of the above pQCD calculations for the magnetic form factor has resulted in the prediction [31]:

$$\frac{B(Q^2)}{A(Q^2)} \simeq \frac{4\tau(\tau+1)}{\tau^2+\tau+3/4} \; , \tag{14}$$

for $Q^2 >> 2M_d\Lambda_{QCD} \sim 0.8$ (GeV/c)^2, which fails to account for the presence of a diffraction minimum in the magnetic form factor. A refinement [32] of the above prediction, which includes helicity-flip matrix elements assumed to be negligible in the original calculation, preserves the asymptotic behavior of the ratio but at the same time allows for the existence of a diffraction minimum in the magnetic form factor.

2 Overview of Large $\mathbf{Q^2}$ Measurements

The unique features of the Continuous Electron Beam Accelerator and Hall A Facilities of JLab offered recently the opportunity to extend the kinematical range of $A(Q^2)$ and to resolve inconsistencies in previous data sets from different laboratories by measuring [6] forward scattering angle elastic electron-deuteron scattering for $0.7 \leq Q^2 \leq 6.0$ (GeV/c)^2. Backward angle measurements [33] in conjunction with the forward angle measurements enabled also determination of $B(Q^2)$ in the kinematical range $0.7 \leq Q^2 \leq 1.4$ (GeV/c)^2. Electron beams were scattered off a liquid deuterium target. Scattered electrons were detected in the electron High Resolution Spectrometer (HRS). To suppress backgrounds and separate elastic from inelastic scattering events, recoil deuterons were detected in coincidence with the scattered electrons in the hadron HRS. A schematic of the Hall A Facility as used in this experiment (E91-26) is shown in Figure 4.

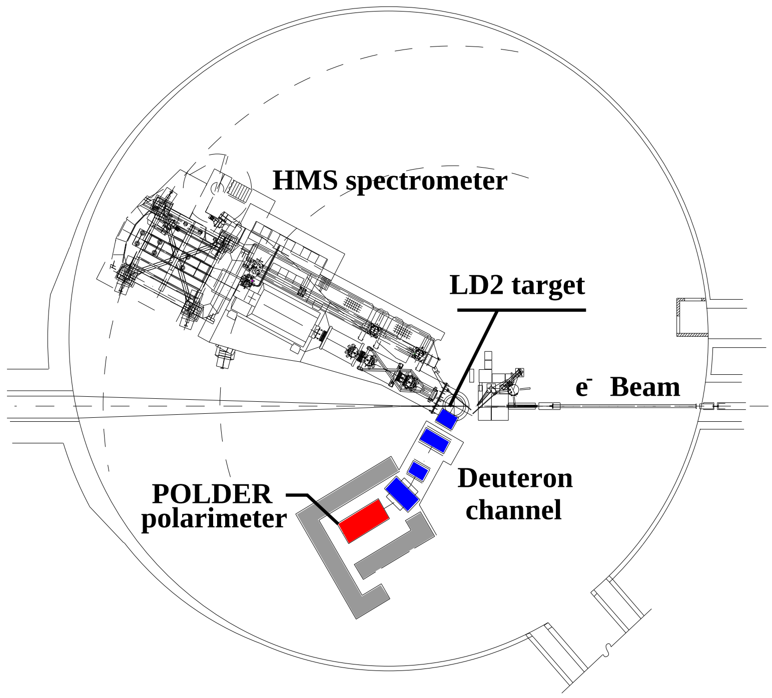

Figure 5: Plan view of the JLab Hall C Facility as used for the recent measurement [11] of the deuteron $t_{20}(Q^2)$. Shown are the electron High Momentum Spectrometer, the deuteron cryotarget, and the recoil deuteron spectrometer with the POLDER polarimeter.

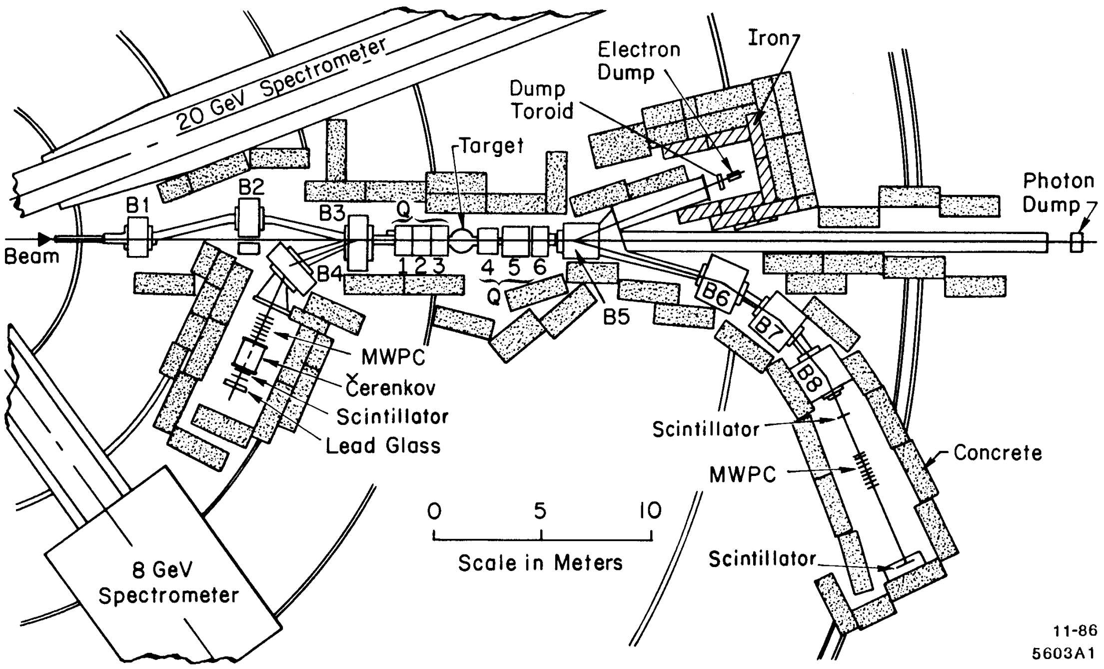

Figure 6: Plan view of the 180° electron and 0° deuteron magnetic spectrometer systems [35, 36] used for the SLAC End Station A measurement [7] of the deuteron $B(Q^2)$ (see text).

Recent advances in deuteron polarimetry and the high luminosity of the JLab Hall C Facility enabled also large Q^2 measurements of $t_{20}(Q^2)$ [11] for $0.7 \leq Q^2 \leq 1.7$ (GeV/c)^2. The experiment (E94-18) also measured precisely $A(Q^2)$ in the same Q^2 region [34]. The experimental setup used the Hall C High Momentum Spectrometer (HMS) to detect scattered electrons and a special deuteron channel to detect and spin-analyze recoil deuterons in coincidence with the electrons (see Figure 5). The deuteron channel consisted of a large solid angle magnetic spectrometer comprised of three quadrupole and one dipole magnets, and the POLDER deuteron tensor polarimeter, calibrated previously at the Saturn Laboratory. The polarimeter was based on the charge exchange reaction $H(\vec{d}, pp)n$ induced by the recoil deuterons in a liquid hydrogen cell. Deuterons incident on the polarimeter were identified with two scintillator trigger planes and two sets of wire chambers. The pairs of protons from the charge exchange reactions were identified with two pairs of scintillator hodoscopes and a wire chamber set.

The highest Q^2 measurements of $B(Q^2)$ were performed [7] in the mid-1980's with a novel double-arm spectrometer system [35, 36] in the SLAC End Station A (Experiment NE4), as shown in Figure 6. Electron beams from the Nuclear Physics Injector were directed on a deuteron target through a chicane of dipole magnets (B1, B2 and B3). Electrons scattered at 180° were transported through a large solid angle spectrometer system consisting of three quadrupole (Q1, Q2, and Q3) and two dipole (B3 and B4) magnets to a set of detectors. Deuterons recoiling at 0° were transported through a spectrometer system consisting of three quadrupole (Q4, Q5, and Q6) and four dipole (B5, B6, B7 and B8) magnets to another set of detectors. The primary (unscattered) beams were directed onto a beam dump located inside the End Station. Elastic electron-deuteron coincidence events were identified by the time-of-flight (TOF) method.

3 Experiment versus Theory

The experimental data for $A(Q^2)$, $B(Q^2)$ and $t_{20}(Q^2)$ are shown (with the exception of recent $t_{20}(Q^2)$ data from Novosibirsk [37]) in Figures 7–10 together with non-relativistic and relativistic theoretical calculations. The data for $A(Q^2)$ indicate a smooth fall off with no apparent diffractive structure. The data for $B(Q^2)$ indicate the presence of a diffraction minimum in the vicinity of $Q^2 = 1.8$ (GeV$/c)^2$. The large error bars of the SLAC NE4 data are due to limited statistics and to systematics associated with a large photoproduction background mimicking elastic electron-deuteron coincidences. The $t_{20}(Q^2)$ data together with the $A(Q^2)$ and $B(Q^2)$ data show that the charge form factor exhibits a diffractive structure with a minimum at $Q^2 = 0.7$ (GeV$/c)^2$ and that the quadrupole form factor falls off exponentially in the measured Q^2 region [11].

Figure 7 shows $A(Q^2)$ and $B(Q^2)$ data for $Q^2 < 2$ (GeV$/c)^2$ compared with a state of the art non-relativistic calculation by Schiavilla and collaborators [38] using the Argonne v_{18} nucleon-nucleon potential. The calculation is based on the impulse approximation approach and includes relativistic corrections and meson-exchange currents. The solid dots in the $B(Q^2)$ plot are the recent data from the JLab E91-26 Hall A experiment [33]. The dashed curve is the impulse approximation calculation. The dot-dashed curve is the full calculation.

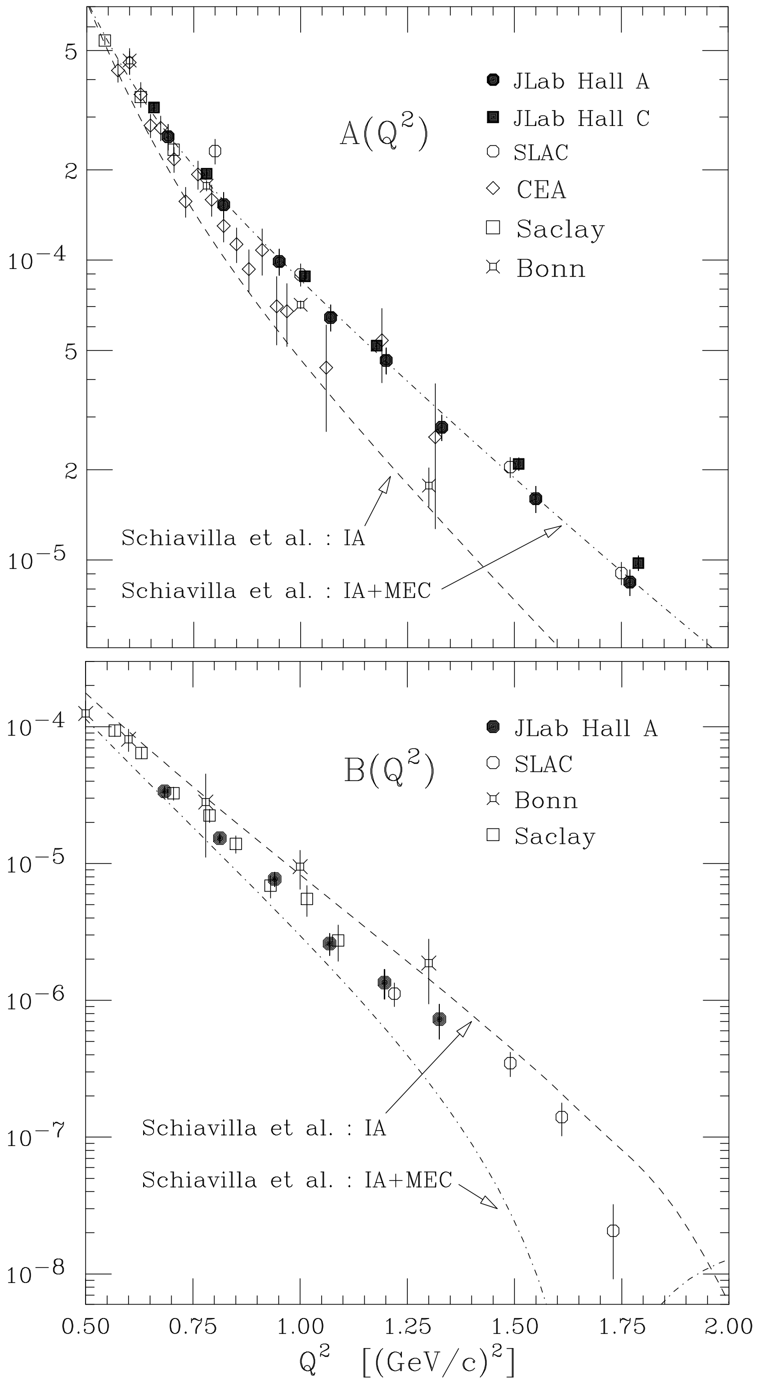

Figure 7: Low Q^2 data [6, 7] on the deuteron $A(Q^2)$ and $B(Q^2)$ electric and magnetic form factors compared with non-relativistic impulse approximation calculations by Schiavilla and collaborators [38] with and without inclusion of meson-exchange currents.

It is evident from the Figure that this non-relativistic calculation cannot describe both form factors at the same time. This is a pattern present in all non-relativistic calculations.

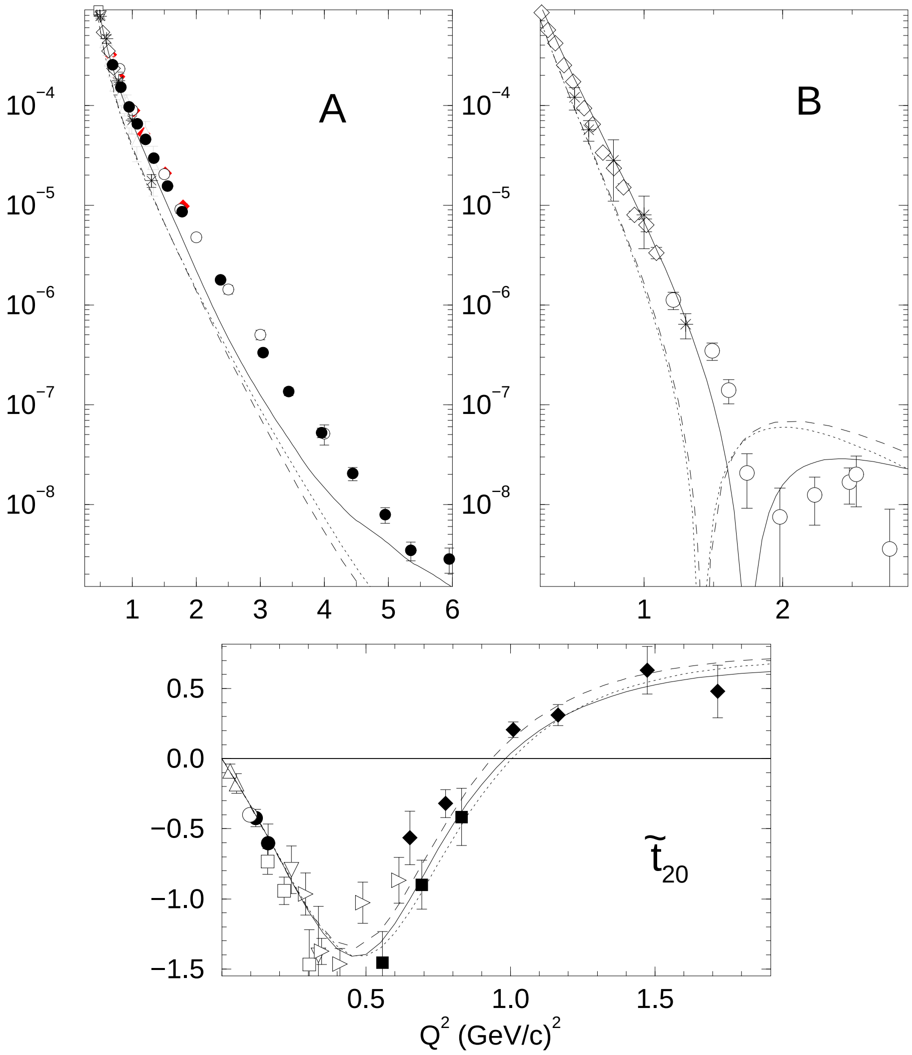

Figure 8: Experimental data [6, 7, 10, 11] on the deuteron $A(Q^2)$, $B(Q^2)$ and $\tilde{t}_{20}(Q^2)$ compared with theoretical calculations based on propagator dynamics (RIA) [20, 21, 22] (see text).

Figure 8 shows all the available $A(Q^2)$, $B(Q^2)$ and $\tilde{t}_{20}(Q^2)$ experimental data and theoretical calculations based on the propagator dynamics approach [sometimes referred to as the relativistic impulse approximation (RIA)] by three different groups. The solid, dotted and dashed curves represent the RIA calculations of Van Orden, Devine and Gross (VDG) [20], Hummel and Tjon (HT) [21], and Phillips, Wallace and Devine (PWD) [22], respectively.

The VDG curve is based on the Gross quasipotential equation [39] with a one-boson-exchange interaction and assumes that the electron interacts with an off-mass-shell nucleon or a nucleon that is on-mass-shell right before or after the interaction (see Figure 2). The HT curve is based on a one-boson-exchange quasipotential approximation of the Bethe-Salpeter equation [40], where the two nucleons are treated symmetrically by putting them equally off their mass-shell with zero relative energy. The PWD curve is also based on a one-boson-exchange interaction but with a single-time equation that constraints the relative time to be zero.

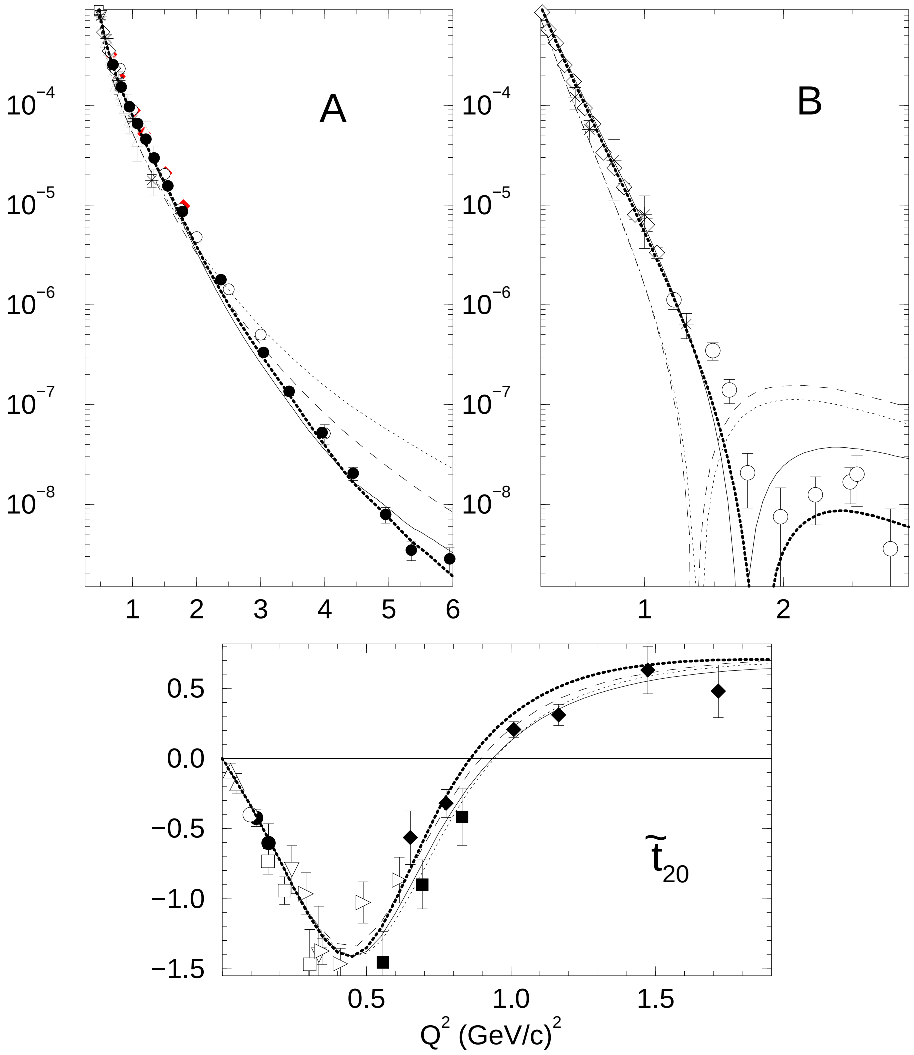

Figure 9: Experimental data [6, 7, 10, 11] on the deuteron $A(Q^2)$, $B(Q^2)$ and $\tilde{t}_{20}(Q^2)$ compared with theoretical calculations based on propagator dynamics (RIA) with inclusion of the $\rho\pi\gamma$ interaction current [20, 21, 22, 23] (see text).

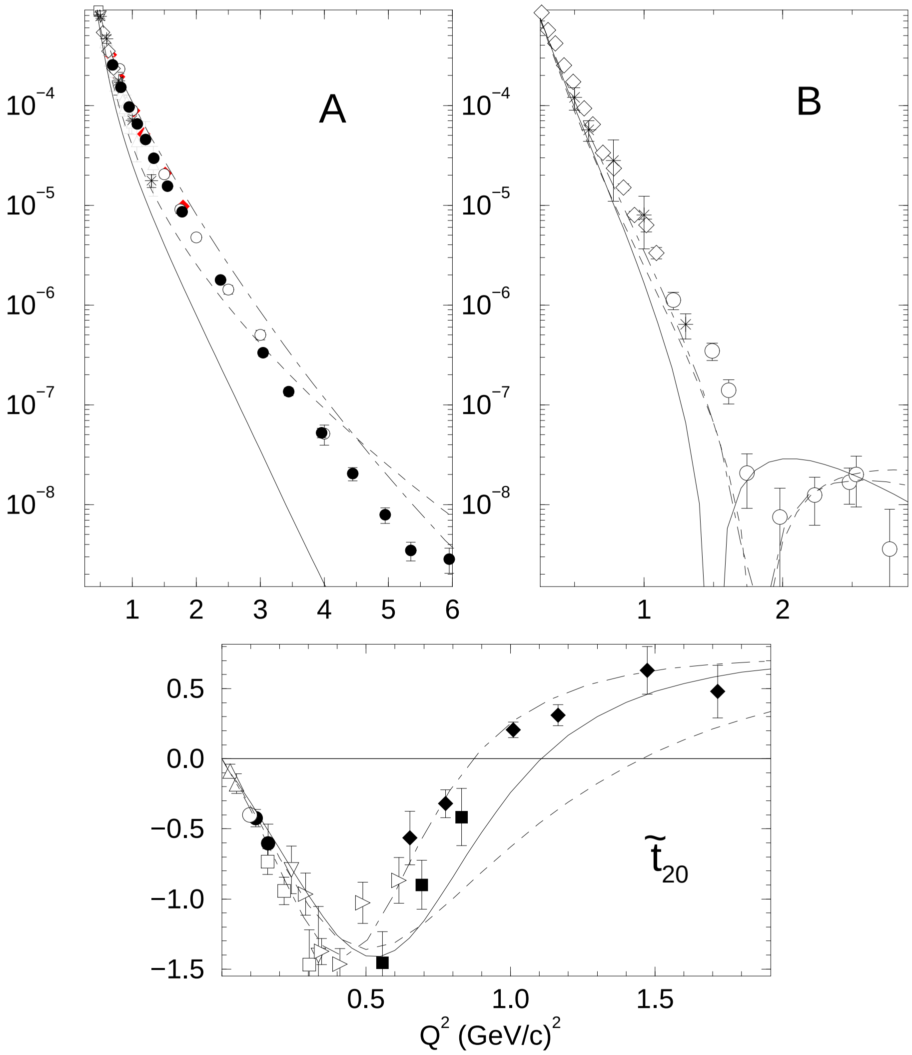

Figure 10: Experimental data [6, 7, 10, 11] on the deuteron $A(Q^2)$, $B(Q^2)$ and $\tilde{t}_{20}(Q^2)$ compared with selected theoretical calculations based on hamiltonian dynamics [42, 43, 44] (see text).

In all three cases the relativistic impulse approximation fails to describe the data. All three theory groups have augmented their models by including the $\rho\pi\gamma$ MEC contribution as shown in Figure 9. The magnitude of this contribution depends on the $\rho\pi\gamma$ coupling constant and vertex form factor choices [41]. The VDG model (solid curve) uses a soft $\rho\pi\gamma$ form factor. The HT model (thin dotted curve) uses a Vector Meson Dominance model hard form factor. The PWD model (dashed curve) uses an intermediate form factor. The inclusion of the $\rho\pi\gamma$ MEC contribution has a small effect on $B(Q^2)$ and $\tilde{t}_{20}(Q^2)$ but increases dramatically

$A(Q^2)$. The $A(Q^2)$ data favor use of the softest possible form factor. The thick dotted curve is an alternate calculation by the VDG group with a different nucleon form factor choice in the off-shell modification of the single nucleon current as required to insure current conservation (see next section). This modification affects significantly $B(Q^2)$ and to a lesser degree $\tilde{t}_{20}(Q^2)$. Although the difference in the models is indicative of the size of theoretical uncertainties and ambiguities, it appears that the relativistic impulse approximation can, as in the case of the alternate VDG model, reproduce the deuteron form factor data fairly well.

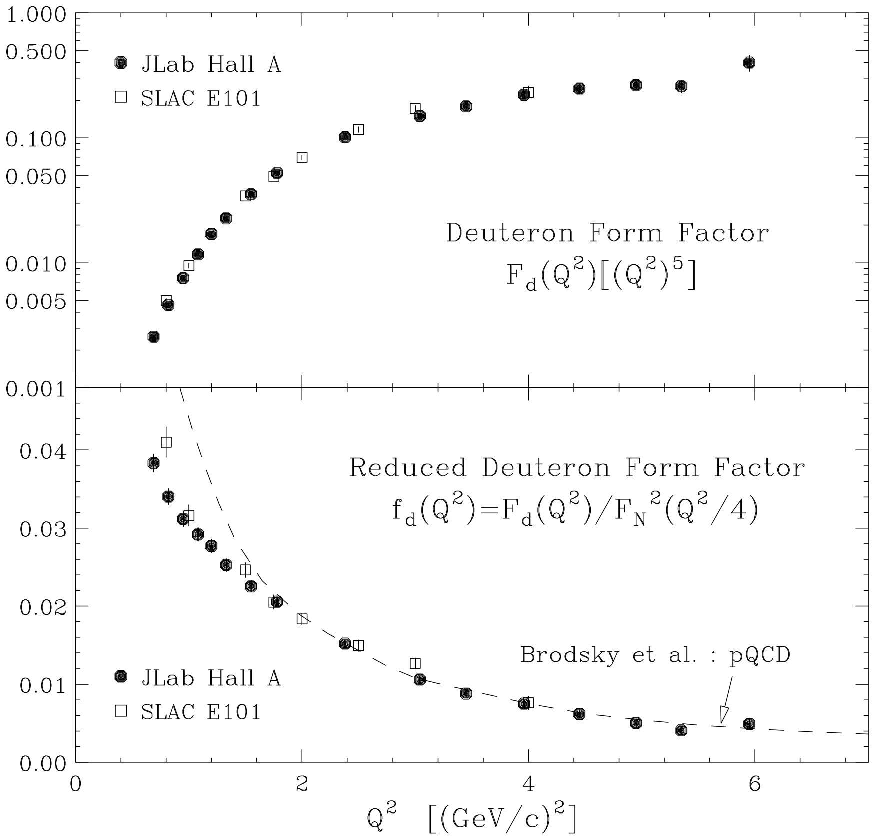

Figure 11: The deuteron form factor $F_d(Q^2)$ times $(Q^2)^5$ (top) and the reduced deuteron form factor $f_d(Q^2)$ (bottom) from JLab [6] and SLAC [45] data. The curve is the asymptotic pQCD prediction [30] for $\Lambda_{QCD} = 100$ MeV, arbitrarily normalized to the data at $Q^2 = 4$ (GeV/c)^2.

Figure 10 shows a comparison of selected recent hamiltonian dynamics calculations with the available experimental $A(Q^2)$, $B(Q^2)$ and $\tilde{t}_{20}(Q^2)$ data. The solid curve is a point form calculation by Allen, Klink and Polyzou [42] using the Argonne v_{18} potential. The dashed curve is a front form calculation by Lev, Pace and Salmè [43] using the Nijmegen potential. The dot-dashed curve is an instant form calculation by Schiavilla and Pandharipande [44] using the Argonne v_{18} potential. These three calculations employ different approaches for the construction of the electromagnetic current. It is evident that none of these admittedly promising approaches is able, at this stage, to describe simultaneously all three $A(Q^2)$, $B(Q^2)$ and $\tilde{t}_{20}(Q^2)$ deuteron observables.

Figure 11 (top) shows values for the "deuteron form factor" $F_d(Q^2) \equiv \sqrt{A(Q^2)}$ from JLab experiment E91-26 [6] and SLAC experiment E101 [45] multiplied by $(Q^2)^5$. It is evident that the data exhibit a behavior consistent with the power law of QDS and pQCD. Figure 11 (bottom) shows values for the "reduced" deuteron form factor $f_d(Q^2) \equiv F_d(Q^2)/F_N^2(Q^2/4)$, where the two powers of the nucleon form factor $F_N(Q^2) = (1 + Q^2/0.71)^{-2}$ remove in a minimal and approximate way the effects of nucleon compositeness [46]. The $f_d(Q^2)$ data appear to follow, for $Q^2 > 2$ (GeV/c)^2, the asymptotic Q^2 prediction of pQCD [30]:

$$f_d(Q^2) \sim \frac{\alpha_s(Q^2)}{Q^2}\left[\ln\frac{Q^2}{\Lambda^2_{QCD}}\right]^{-\Gamma}. \tag{15}$$

Here $\Gamma = -(2C_F/5\beta)$, where $C_F = (n_c^2 - 1)/2n_c$, $\beta = 11 - (2/3)n_f$, with $n_c = 3$ and $n_f = 2$ being the numbers of QCD colors and effective flavors. Although several authors have questioned the validity of QDS and pQCD at the momentum transfers of the JLab experiment [47, 48], similar scaling behavior has been reported in deuteron photodisintegration at moderate photon energies [49]. New large momentum transfer data on many observables, including the deuteron magnetic form factor as well as the three- and four-body form factors will be necessary, before drawing any definitive conclusion for the applicability of pQCD in exclusive processes in the kinematical domain accessible by today's machines.

4 Motivation for New B(Q^2) Measurements

Jefferson Lab is the ideal place to study experimentally the deuteron form factors, "observables of choice" [50] for testing meson-nucleon models describing the electromagnetic structure of the deuteron. The unique capability of its high luminosity and the availability of its superior resolution large acceptance magnetic spectrometers, were instrumental in extending, with an unprecedented precision, the measurements of the deuteron electric form factor $A(Q^2)$ and tensor polarization $t_{20}(Q^2)$ to momentum transfers not accessible by other electron machines. The same features of JLab can by utilized to study the diffraction minimum and the secondary maximum of the deuteron magnetic form factor $B(Q^2)$, and probably more than double the Q^2 range of the existing $B(Q^2)$ data.

The $B(Q^2)$ SLAC data acquired in the "heroic effort" [3] of SLAC experiment NE4 uncovered the diffractive feature of $B(Q^2)$ predicted by the theory (although not beyond *any doubt*, as has been stressed in Ref. [3]) but were unable to determine reliably the location of its diffraction minimum and the strength of its secondary maximum. The NE4 results were limited by large statistical uncertainties, and large systematic uncertainties from an unexpected large background from two-step photoproduction processes in the target. This background was attributed [7] to electron-deuteron coincidences from $\gamma d \to \gamma d$ and/or $\gamma d \to \pi_o d$ reactions initiated by bremsstrahlung photons in the target. The second reaction also results in photon production as the π_o decays in the target into two photons. In both cases the outcome was the coincidence between a deuteron in the recoil spectrometer and an electron in the electron spectrometer, originating from pair production of a final state photon in the target. The effect of this unforeseen background, which mimicked elastic coincidence events, was inadvertently magnified by the long targets used in NE4 and by the poor resolution of the recoil spectrometer. The effect of this background is shown, for the presence of the $\gamma d \to \gamma d$ reaction only, in Figure 12, where spectra of coincidence events are plotted for nine different kinematics versus the double-arm missing momentum δ_{mm} defined as the sum of the relative electron and deuteron momenta (with respect to the central electron and deuteron spectrometer momenta). JLab can overcome the limitations of the SLAC experiment by using in a high luminosity experiment a short target and a recoil spectrometer with very good resolution as the hadron HRS.

It is well known that the deuteron magnetic form factor is extremely sensitive to the details of the theoretical calculations [1, 2, 3]. All non-relativistic calculations show a large sensitivity in the nucleon-nucleon potential used, the modeling in the inclusion of MEC and the possible admixtures of nucleon isobars and six-quark states in the deuteron wave function. Small variations of unconstrained parameters of the models result in big differences

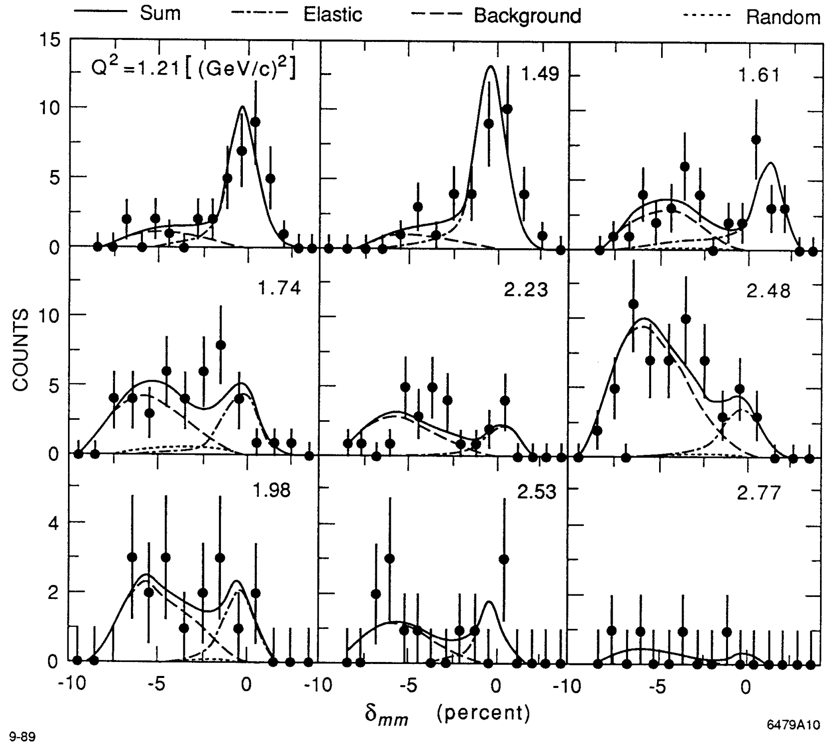

Figure 12: Spectra of elastic electron-deuteron coincidence events versus missing momentum for nine Q^2 kinematics from SLAC experiment NE4 [7] (see text). The data were fitted to a sum of three curves: elastic scattering, selected photoproduction background, and random background. The shapes of the elastic and background curves were determined by Monte Carlo simulation.

in the location of the diffraction minimum of $B(Q^2)$ and the strength and Q^2 evolution of the secondary maximum. Typical examples on this sensitivity can be found in Refs. [2], [14], [27] and [38]. A similar degree of sensitivity is observed in the relativistic calculations using hamiltonian dynamics or propagator dynamics as it is evident by inspection of Figures 8, 9 and 10 (see also Ref. [51]).

In the most complete study of the deuteron form factors using propagator dynamics with the Gross equation, the VDG group observed that $B(Q^2)$ is extremely sensitive to the presence of small P-state components of the deuteron wave function of relativistic origin. In particular, the position of the minimum of $B(Q^2)$ is very sensitive to the sign of the singlet P state v_s. This observation is very surprising, because the probability of the v_s state is only

0.01%. The reason such a small component can have such a large effect is due to a double interference between the small P states and the larger S- and D-state components. This is easily seen when one considers the decomposition of the magnetic form factor in electric and magnetic parts (similarly to the non-relativistic impulse approximation case):

$$G_M = (G_E^p + G_E^n) D_M^E + (G_M^p + G_M^n) D_M^M, \tag{16}$$

and obtains, to first order in $(Q/M)^2$, the low-Q^2 limit for the relativistic impulse approximation:

$$\begin{aligned} D_M^E &= \int_0^\infty dr\, \frac{3}{2} w^2(r) + \frac{2Mr}{\sqrt{3}} \left[v_t(r) \left(\frac{1}{\sqrt{2}} u(r) - w(r) \right) \right. \\ &\quad \left. \left. - v_s(r) \left(u(r) + \frac{1}{\sqrt{2}} w(r) \right) \right] \right\} [j_0(k) + j_2(k)] \ , \qquad (17) \\ D_M^M &= \int_0^\infty dr \left[\left(2u^2(r) - w^2(r) \right) j_0(k) + \left(\sqrt{2} u(r) w(r) + w^2(r) \right) j_2(k) \right] \ , \qquad (18) \end{aligned}$$

where v_t is the triplet P state of the relativistic four-component deuteron wave function. All terms quadratic in the P states are very small in this region but the small P components of the terms in D_M^E interfere with the large components, enhancing the overall effect of the small components. Also if the sign of the v_s component is opposite to that of v_t, the two separate interference terms will add coherently enhancing their effect.

Another source of uncertainty in the VDG model is the off-shell modification of the single-nucleon current. This is necessary to insure current conservation, by satisfying the Ward-Takahashi identity. The VDG solution of this constraint results in a nucleon electromagnetic current requiring an unconstrained form factor, $F_3(Q^2)$, in addition to the Dirac and Pauli form factors $F_1(Q^2)$ and $F_2(Q^2)$, and three associated, partly constrained, functions of the off-shell virtuality of the nucleon. Recent studies by Van Orden and Gross [23, 24] have shown that the secondary maximum of $B(Q^2)$ is very sensitive to the hardness of the $F_3(Q^2)$ off-shell form factor and that reasonable variations in the $F_3(Q^2)$ choices have a small effect in $\tilde{t}_{20}(Q^2)$ and minimal effect on $A(Q^2)$. This can be seen by comparing the curves of Figures 8 and 9. The solid curve of Figure 9 uses a dipole-type form for the $F_3(Q^2)$ form factor meanwhile the thick-dotted curve uses a tripole-type form.

A third source of uncertainty in the VDG model is the hardness of the $\rho\pi\gamma$ form factor. The particular choice for this form factor has a large effect on $A(Q^2)$ but a small effect on $B(Q^2)$ and almost no effect in $\tilde{t}_{20}(Q^2)$, as can be seen by examination of Figures 8 and 9, given that the VDG, HT and PWD groups use significantly different $\rho\pi\gamma$ form factor choices. Since the above three uncertainties affect primarily three different aspects of the data, namely the location of the $B(Q^2)$ diffraction minimum, the height of the secondary maximum of $B(Q^2)$ and its evolution to larger Q^2, and the overall magnitude of $A(Q^2)$, a precise measurement of the location of the diffraction minimum and of the height and shape of the secondary maximum of $B(Q^2)$ will constrain the theoretical model and provide a consistent description of both elastic form factors $A(Q^2)$ and $B(Q^2)$.

The importance of precise $B(Q^2)$ measurements in discriminating among the differing theoretical calculations is demonstrated in Figure 13, which contains a representative sample of recent propagator and hamiltonian dynamics calculations and an older quark-cluster hybrid model calculation compared to $A(Q^2)$, $B(Q^2)$ and $t_{20}(Q^2)$ data. The theory curves in the Figure are, in order of the Q^2 of their minima in $B(Q^2)$, by: Carbonnel and Karmanov [52] (hamiltonian dynamics/front-form, long dot-dashed line); Phillips, Wallace and Devine [22] (propagator dynamics, dashed double-dotted line); Allen, Klink and Polyzou [42](hamiltonian dynamics/point-form, short dot-dashed line); Van Orden and Gross [23, 24] (propagator dynamics/full calculation, solid line); Van Orden, Devine and Gross [23, 24] (propagator dynamics/RIA only, long dashed line); Lev, Pace and Salmè [43] (hamiltonian dynamics/front-form, dotted line); Dijk and Bakker [27] (quark-cluster hybrid, widely spaced dotted line); Schiavilla and Pandharipande [44] (hamiltonian dynamics/instant form, medium dashed line); and Arenhövel, Ritz and Wilbois [53] (hamiltonian dynamics, short dashed line). The *"most striking feature of this plot is the large model dependence of the predictions for $B(Q^2)$"*, as has been stressed in the review work of Ref. [3]. A new precise measurement of $B(Q^2)$ can obviously provide severe constraints in the parameters of the calculations with an unprecedented discriminative power. The second obvious striking feature of the plot are the large error bars of the higher Q^2 data of $B(Q^2)$ that offer a limited discriminative power, necessitating the need for new precise measurements.

The pQCD calculations predict fairly large values for $B(Q^2)$ for $Q^2 > 2.5$ (GeV/c)^2, easily measurable in a JLab experiment. The expected values are significantly larger than the ones predicted by conventional non-relativistic or relativistic meson-nucleon calculations.

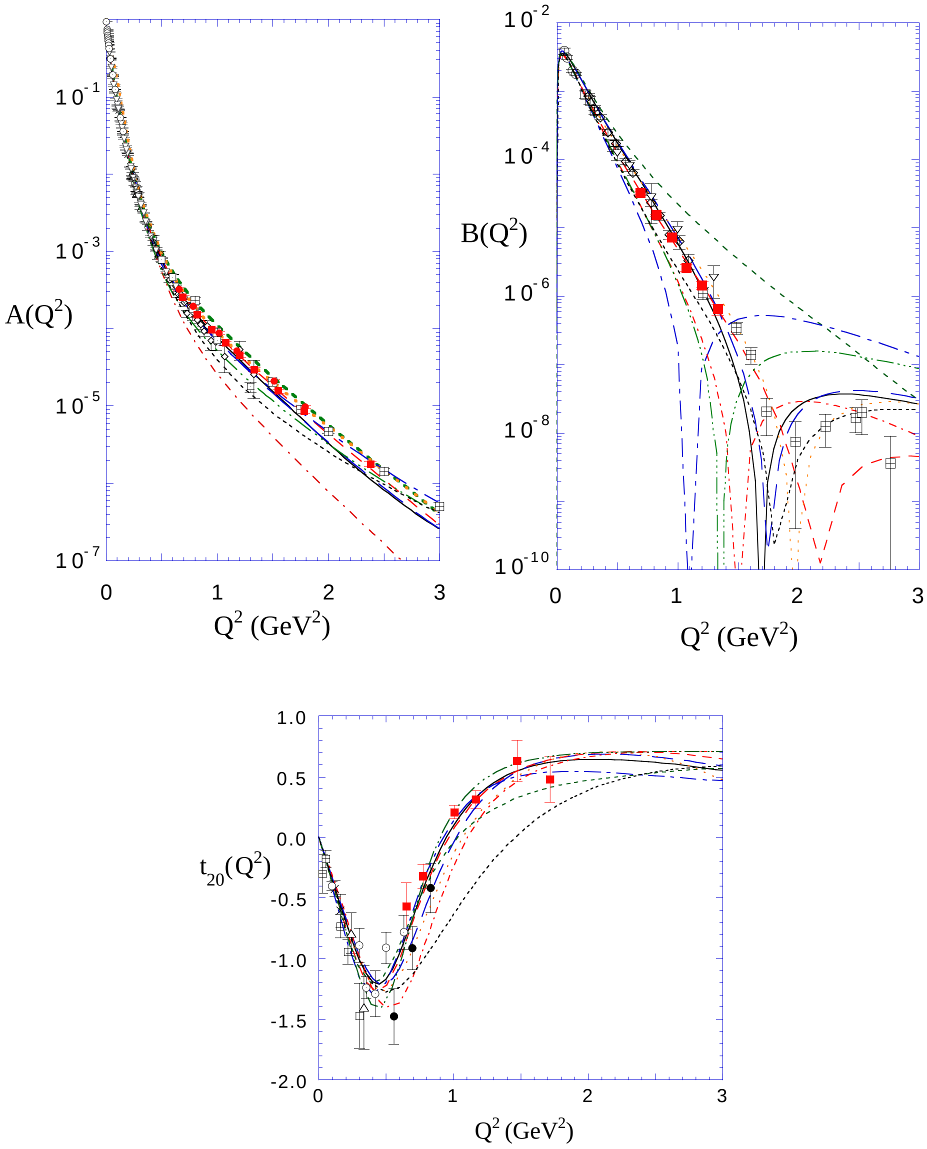

Figure 13: Comparison of available deuteron $A(Q^2)$, $B(Q^2)$ and $t_{20}(Q^2)$ data [6, 7, 10, 11] with selected theoretical calculations [22, 23, 27, 42, 43, 44, 52, 53] (see text). Of note is the large model dependence of the predictions for $B(Q^2)$.

The original pQCD prediction for the ratio $B(Q^2)/A(Q^2)$ by Brodsky and Hiller [31] and its improvement by Kobushkin and Syamtomov [32] are shown in Figure 14. Shown also in the Figure are data from SLAC [7], Bonn [54] and Saclay [55]. A new JLab experiment will offer large Q^2 $B(Q^2)$ data that can provide some finality to the, unresolved for more than a quarter of a century, issue of the applicability of pQCD to the deuteron form factor description and either validate the apparent success of QDS and pQCD in describing $A(Q^2)$, or put it to rest.

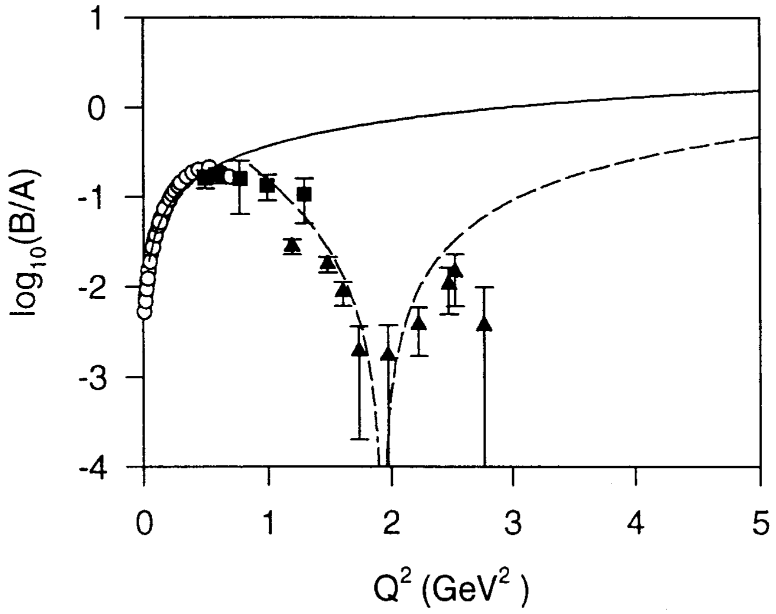

Figure 14: Perturbative QCD predictions for the deuteron $A(Q^2)/B(Q^2)$ ratio. The solid curve is the original calculation by Brodsky and Hiller [31]; the dashed curve includes a correction of order Λ_{QCD}/M_d by Kobushkin and Syamtomov [32]. The data are from SLAC [7] (solid triangles), Bonn [54] (solid squares) and Saclay [55] (open circles).

It should be noted that there has been a tremendous amount of theoretical work on the deuteron form factors in the last decade and in particular after the publication of the JLab $A(Q^2)$ and $t_{20}(Q^2)$ data. A successful completion of this work will require new improved data on the deuteron $B(Q^2)$ over the Q^2 region of its apparent diffraction minimum and beyond to larger Q^2 to constrain remaining theoretical uncertainties. A JLab measurement of the deuteron $B(Q^2)$ with a precision comparable to the previous $A(Q^2)$ JLab measurements will significantly advance our understanding of the internal structure and dynamics of the deuteron, and quite possibly *establish a canonical consistent hadronic model describing the electromagnetic structure of the deuteron.*

The importance of the previous SLAC and JLab experiments on the deuteron form factors for our understanding of the simplest nucleus in nature is universally accepted. Both the 1990 DOE/NSF Long Range Plan by NSAC [56], which proceeded the SLAC NE4 experiment, and the 2002 Long Range Plan [57], which proceeded the JLab experiments, acknowledged the deuteron form factor measurements as major nuclear physics achievements and called their extensions to the highest momentum transfers possible as essential for the advancement of nuclear physics. While the extension of $A(Q^2)$ [58] will have to wait for the 12 GeV upgrade of JLab and the extension of $t_{20}(Q^2)$ for a major new idea in deuteron polarimetry, the extension of $B(Q^2)$ is presently feasible at JLab.

We are proposing to perform the much needed extension of $B(Q^2)$ by reaching the limits of magnetic elastic scattering from the deuteron accessible by the unique features of JLab. Our objective is to improve significantly the quality of the existing data on the deuteron $B(Q^2)$ around its diffraction minimum and extend the existing measurements to the highest momentum transfers, possibly up to $Q^2 = 6$ (GeV/c)^2, limited only by cross section sensitivity of one elastic event per day [as in the JLab E91-26 experiment on $A(Q^2)$]. The new data will be of significant importance for the development of a canonical theory based on hadronic degrees of freedom describing the electromagnetic structure of the deuteron.

5 The Experiment

The existing deuteron form factor data show that, for $Q^2 > 1.5$ (GeV/c)^2, the electric form factor is 2 to 3 orders of magnitude greater than the magnetic one, dictating that *any future $B(Q^2)$ measurements for $Q^2 > 1.5$ (GeV/c)^2 must be performed around 180°* so that the contributions from $A(Q^2)$ would not dominate the elastic cross section.

The cross section to be measured is known to be small and of the order of 10^{-41} to 10^{-42} cm^2/sr in the vicinity of the diffraction minimum and beyond, necessitating a good resolution 180° electron magnetic spectrometer with the largest possible solid angle, and the longest possible target consistent with cryogenic limitations and suppression of the expected photoproduction background. The use of a long target introduces large energy losses to the incident and back-scattered electrons and degrades the missing mass resolution. This degradation, being much greater that the 2.2 MeV binding energy of the deuteron, does not allow for the separation of elastic scattering events from inelastic ones, and therefore requires that the recoil deuterons should be detected in coincidence in a 0° magnetic spectrometer.

The 180° electron spectrometer system and a required magnet chicane for transporting the incident beam onto the target can be built from existing magnets at JLab or at other National Laboratories such as SLAC. The hadron (left) HRS of Hall A is the ideal choice for the required 0° recoil spectrometer system in conjunction with a chicane of dipole magnets for transporting the incident electrons to the beam dump.

The identification of the electron-deuteron coincidences will rely on double-arm TOF measurements. The double-arm electron-deuteron coincidences from the two-step photo-production background processes observed in SLAC experiment NE4 will be significantly suppressed in this experiment. This background, being at least proportional to the square of the target length, will be significantly reduced by using a target length of 10 cm, much shorter than the 20 and 40 cm target lengths used at SLAC. The resolutions of the electron and in particular of the recoil spectrometer will provide application of strict cuts in the angular correlation of the scattered and recoil particles (not applied in the SLAC experiment because of the poor resolution of its recoil spectrometer) resulting in further rejection of any background events from these two-step processes.

The calibration of the entire double-arm system will rely on careful magnetic measurements of the non-HRS spectrometer magnets and will be checked with elastic electron-proton scattering in coincidence. Elastic scattering from hydrogen will be measured at every kinematical point of the elastic deuteron scattering. The most important check will be the confirmation of our knowledge of the double-arm solid angle for the elastic deuteron measurements. The double-arm solid angle will be calculated by means of Monte Carlo simulation as was done for the SLAC NE4 experiment on $B(Q^2)$ and for the JLab E91-26 Hall A experiment on $A(Q^2)$. Details on the simulation method can be found in Refs. [35] and [59]. The proposed experimental setup will be also able to provide precision measurements of the proton magnetic form factor at large momentum transfers. The advantage of these 180° measurements will be the absence of the well known experimental deficiencies of Rosenbluth separations using data from different scattering angles.

The experiment will require new target cells for the deuterium and proton targets. The optimum target length for reducing the two-step background by at least a factor of four as compared to the SLAC experiment is 10 cm. The angular acceptance of the scattered electrons is very large, requiring that the diameter of the cells should be ~6 cm so that the back-scattered electrons do not pass through the cell walls. The tested cooling capability of Hall A will allow use of beam currents as high as 150μA, with a tolerable dissipated power of ~680 W. Beam-intensity induced changes in the density of liquid hydrogen and deuterium targets have been measured to be, under similar conditions in Hall A, on the order of a few percent, resulting in a fractional cross section error of $\sim 0.5\%$.

5.1 The 180°/0° Spectrometer System

Our proposed 180°/0° double-arm spectrometer system is essentially identical to the system designed for the original 1991 JLab E91-26 proposal [60] on large Q^2 measurements of the deuteron $A(Q^2)$ and $B(Q^2)$ and partly similar to that used in SLAC experiment NE4, and is shown schematically in Figure 15. The incident electron beam travels, after exiting the Hall A tunnel, through the chicane of dipole magnets D2–D3–D4 and then through the magnetic axis of the quadrupole doublet Q4–Q5 before impinging on the target. The back-scattered electrons are focused in the quadrupole doublet Q4–Q5 and momentum analyzed and transported to a set of detectors by the dipole magnets D4–D5.

In order to be able to use the hadron HRS spectrometer with its permanent pointing to the Hall A target pivot center, the target assembly is moved ~1.0 m upstream from its nominal position on the Hall A pivot so that the nominal target center becomes the center of the "split" dipole magnet D6, as shown in Figure 16. To maximize the solid angle of the electron spectrometer, a new scattering chamber with the shortest possible diameter should be used. The optimum diameter that would match the available solid angle by the 180° spectrometer is approximately 50 cm.

The recoil deuterons or protons are deflected towards the Hall A hadron HRS spectrometer by the split dipole magnet D6, as shown in Figure 16. This magnet becomes an additional element of the HRS system, necessitating a minor adjustment to the optics parameters of

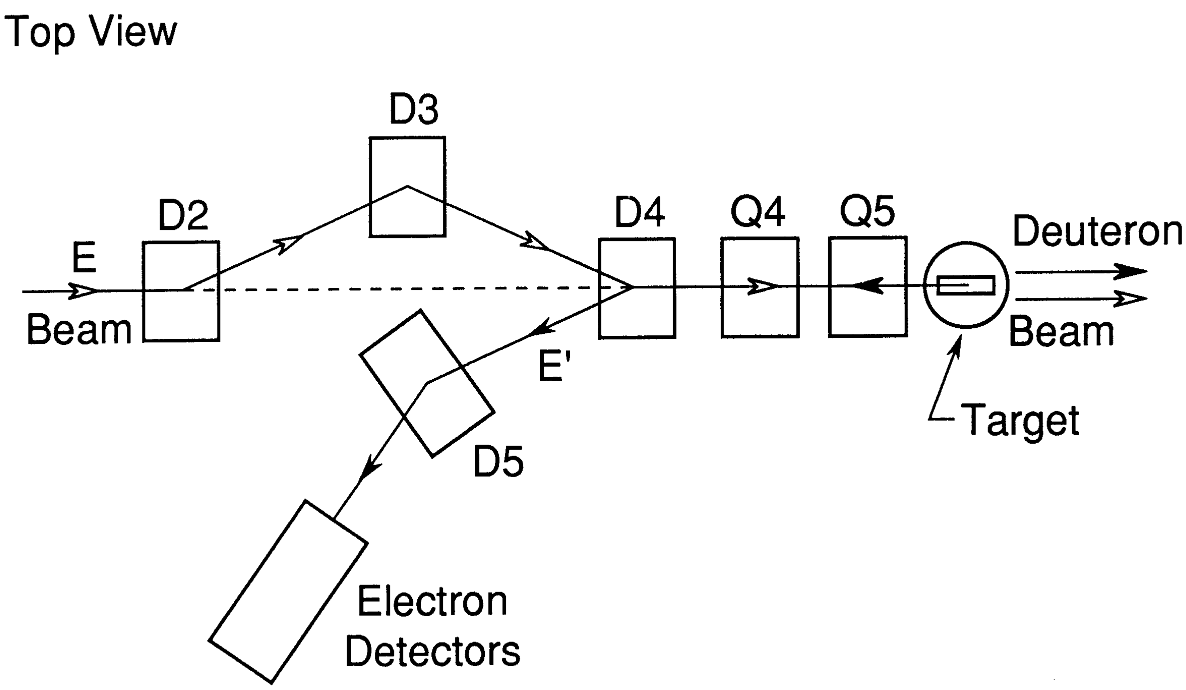

Figure 15: Schematic of the 180° electron spectrometer system and of the incident beam chicane. The elements Q4, Q5 are quadrupole and D2–D5 are dipole magnets. The open arrows pointing to the right indicate the path of the incident electron beam. The solid arrows pointing to the left indicate the central trajectory of the back-scattered electrons.

the HRS (see below). The transmitted beam, which is degraded by radiation, ionization and multiple scattering, is directed towards the beam dump of the Hall through the chicane of dipole magnets D6–D7–D8.

5.1.1 The 180° Electron Spectrometer

To maximize the solid angle of the electron spectrometer, quadrupoles with the shortest possible length and the largest possible aperture should be used. These requirements are best met by the unique capabilities and characteristics of the two quadrupoles of the JLab HKS Hall C spectrometer for hypernuclear studies [61]. Quadrupole Q5 has a radius of 12 cm and a length of 70 cm. Quadrupole Q4 has a radius of 16 cm and a length of 50 cm. The maximum magnetic field of both quads at their poles is 1.6 T. The two dipole magnets

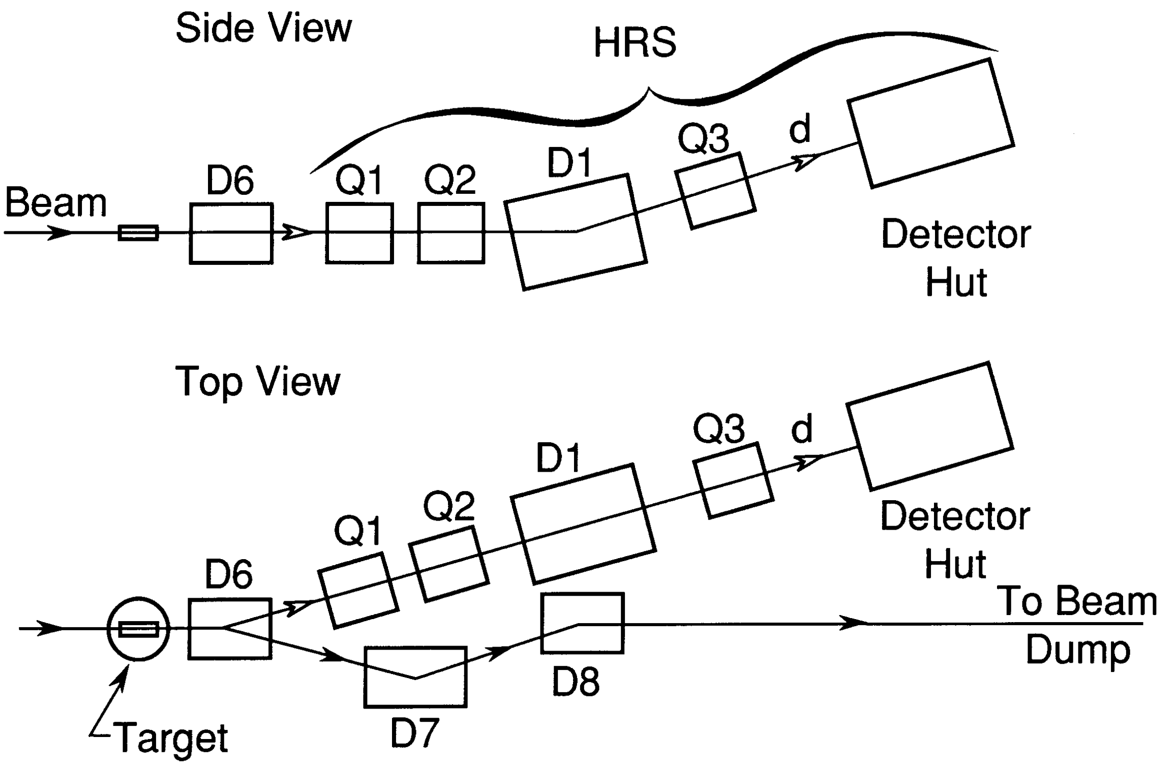

Figure 16: Schematic of the hadron HRS based 0° recoil deuteron spectrometer system, and the exit beam chicane. The elements Q1–Q3 are quadrupole and the elements D1, D6–D8 are dipole magnets. The open arrows indicate the central trajectory of the recoiling deuterons and the solid arrows the path of the electron beam after passing through the target.

D4 and D5 should be of fairly good magnetic field uniformity to fulfill the modest resolution requirements of the elastic deuteron and proton measurements. The gap apertures required to preserve the gathering power of the quadrupoles are small, allowing for several types of surplus dipoles to be used. These two magnets can, in principle, be run in series by a single power supply. An integrated magnetic field of about 0.9 T·m for each one of D4 and D5 will provide a combined bending angle of about 50° for the scattered electrons, which will be sufficient to put the detectors fairly away from the beam line and provide adequate space for their shielding from room background.

The detailed tune of the magnetic fields of the quadrupole doublet Q4 and Q5 will depend on the apertures of the gaps of the two dipole magnets D4 and D5. The magnitude of the two fields will be chosen to maximize the solid angle of the electron spectrometer and at the same time provide sufficient missing mass resolution to separate elastic events from inelastic ones for proton scattering. The angular and momentum resolutions of the $180°$ spectrometer will be dominated by multiple scattering in the target rather than by the quadrupole optics tune. A preliminary study has shown that this proposed system will achieve a solid angle of 30 msr, with a vertical angular acceptance of 200 mr and a horizontal angular acceptance of 50 mr. Knowledge of the solid angle of the spectrometer will require extensive magnetic measurements of its magnetic elements, and proper collimation.

The electron detection package will use the electron HRS detector package consisting of a drift chamber set for the momentum and angular reconstruction of the scattered particles, a Čerenkov counter and a segmented electromagnetic calorimeter for electron identification, and two planes of scintillation hodoscopes for triggering and TOF measurements. The candidate electron signal used for triggering and for double-arm TOF measurements will be the coincidence of the signals of the two scintillator hodoscopes. The detectors should be enclosed in a concrete hut to protect them from room background.

5.1.2 The $0°$ Recoil Spectrometer

The recoiling deuterons will be detected in the Hall A hadron HRS after being deflected by the split magnet D6. The HRS will be at a fixed angle of $10.5°$, pointing at the center of magnet D6. This, smaller than nominal, minimum HRS angle can be achieved by using the hadron HRS in its small angle configuration, where the Q1–Q2 quadrupoles are pushed downstream by $\sim$0.9 m towards the HRS dipole magnet D1. This configuration will require a simple change in the magnetic fields of the Q1–Q3 quadrupole triplet of HRS. The original study [62] of this configuration, with Q1 and Q2 pushed downstream by 1.0 m, has shown that a solid angle of 4 msr can be achieved, with a vertical angular acceptance of 50 mr and a horizontal angular acceptance of 25 mr. The momentum resolution of this configuration is reduced as compared to the one of the standard HRS tune but it is still better than the one needed for our proposed elastic measurements. The angular resolutions are comparable to those of the standard tune and are more than sufficient for the needs of this experiment.

In order to match the solid angle of the deuteron arm with that of the electron arm, the split magnet D6 should be as short as possible, preferably of the standard 36 in. length of surplus magnets. This length limits the D6 maximum deflection angle to about 10.5°, necessitating the small angle configuration of the hadron HRS, but at the same time simplifies greatly the choice and availability of the magnets D7 and D8 needed for the completion of the downstream beam chicane (see below).

The gap of magnet D6 in the vertical direction should be about 15 cm, not limiting the 50 mr angular acceptance of the hadron HRS. The width of the magnet should be large enough to accommodate both mutually diverging beams of recoiling nuclei and incident beam electrons. For a standard surplus magnet length of 36 in. the required width is 35 cm. This makes both types of 18D36 and 29D36 surplus dipole magnets as satisfactory choices for the split magnet D6. Both types of magnets can provide the integrated magnetic field of 1.8 T·m required to deflect the deuterons by 10.5° at the highest Q^2 kinematics of the experiment.

The deuteron detection will require a subset of the full hadron HRS detector package. The two planes of scintillators and the drift chambers will suffice for TOF measurements and for the reconstruction of the recoil nucleus momentum and recoil angle. The candidate deuteron signal used for triggering and for double-arm TOF measurements will be formed by the coincidence of the signals of the two scintillator planes. Knowledge of the recoil spectrometer solid angle and optics will require extensive magnetic measurements for D6, and proper collimation, which is also needed for bremsstrahlung photon background suppression.

5.1.3 The Beam Chicanes

The incident electron beam, after exiting the beam switchyard, is transmitted to the target through the upstream chicane of D2–D3–D4 dipoles. Magnet D2 deflects the beam by the same angle as D4. Magnet D3 is placed symmetrically along the beam path with respect to D2 and D4, and its deflection angle is twice the deflection angle of magnet D2 or D4. The symmetric arrangement and operation of this chicane preserves the initial achromaticity of the electron beam. The horizontal position of D3 is adjusted as necessary to accommodate different kinematical settings. The integrated magnetic field requirement for D2 is the same as of D4, about 0.9 T·m, and for D3 is 1.8 T·m, twice that of D2 or D4. A standard surplus 18D36 bending magnet will be the ideal choice for D4, as was for SLAC experiment NE4.

The incident electron beam after passing through the target will be directed to the beam dump of Hall A through the downstream chicane of dipole magnets D6–D7–D8. Magnet D8 deflects the beam by the same amount as D6. Magnet D7 is placed symmetrically along the beam path with respect to D6 and D8, and its deflection angle is twice the deflection angle of magnet D6 or D8. The horizontal position of D7 is also adjusted to accommodate different beam energies. This chicane is also an achromatic magnet system so that the position and divergence of the electrons at the exit of the chicane do not depend on their momentum. The phase space of the beam going to the dump after exiting D8 will be the same as in an ordinary electron scattering experiment with the beam going straight from the target to the dump. Dipole D8 should have the same integrated magnetic field as D6, preferably of a surplus 18D36 type. Dipole D7 will have to be twice as strong as D6 or D8, providing an integrated magnetic field of 3.6 T·m. A surplus 18D72 dipole can provide this field, as well as the horizontal aperture required to accomodate the phase space of the degraded beam.

A small fraction of the, degraded by bremsstrahlung and ionization energy losses in the target, beam will be deflected onto the vacuum pipe walls of the downstream chicane and onto possible apparatus protection collimators. The deposited power is of the order of a few kW and will require part of the chicane vacuum pipe and collimators to be water cooled as was done recently for the downstream beam chicane of SLAC experiment E158 [63]. Care should be taken of the bremsstrahlung photons emitted along the beam direction in the target. As in the SLAC NE4 experiment, these photons can be absorbed in a small photon dump placed downstream of the target. Proper shielding of the downstream chicane and of the photon dump will be necessary to minimize detector-directed background created in them.

The SLAC NE4 experience suggests that an efficient operation of the two beam chicanes will require extra beam position monitors and fluorescent screens to be placed in strategic points along the beam path, in addition to the existing ones. The information from the beam monitors will be used for minor adjustments to the currents of magnets D2–D3 and D7–D8 in order to align the beam on the axis of each chicane and on its nominal axis towards the beam dump. It is expected that the configuration changes of both chicanes for each proton or deuteron kinematics will dominate the overhead of the running time of the experiment.

6 Kinematics and Run Plan

The kinematical parameters of 180° elastic electron-deuteron scattering in coincidence are given, for the Q^2 range from 1.0 to 6.0 (GeV/c)^2, in Table 1. The last column in the Table is the ratio of the electron to deuteron differential solid angle elements (Jacobian transformation of the solid angle for recoil detection).

To estimate the counting rates and required beam times we have assumed a beam current of 150 μA, a liquid deuterium target length of 10 cm, an electron spectrometer solid angle of 30 msr, a recoil spectrometer solid angle of 4 msr, and a radiative correction factor of 0.7. The cross section values used for $Q^2 \geq 2.5$ (GeV/c)^2 assume a magnetic form factor behavior that follows the general trend of most recent relativistic calculations. The estimated cross section values, counting rates, running times and projected uncertainties in the extraction of $B(Q^2)$ are given in Table 2. The magnetic form factor error, $\Delta B(Q^2)$, includes both statistical and systematic uncertainties. The overall elastic deuteron cross section systematic uncertainty is estimated to be ~4% and is dominated by nuclear interactions of the recoil deuterons in the target and the detectors, and by the uncertainty in the double-arm solid angle. The uncertainty of the previously measured $A(Q^2)$ has been also included in the calculation. In the Q^2 region around the $B(Q^2)$ diffraction minimum the later uncertainty dominates $\Delta B(Q^2)$ and has been estimated to be ~5%, based on the existing $A(Q^2)$ JLab [6, 34] and SLAC [45] measurements. The quality of the projected data possible from this proposed experiment is shown, for the above assumptions, in Figure 17. It is evident from the Figure that the proposed $B(Q^2)$ data will be of unprecedented precision, comparable to the precision of the previous $A(Q^2)$ and $t_{20}(Q^2)$ JLab data.

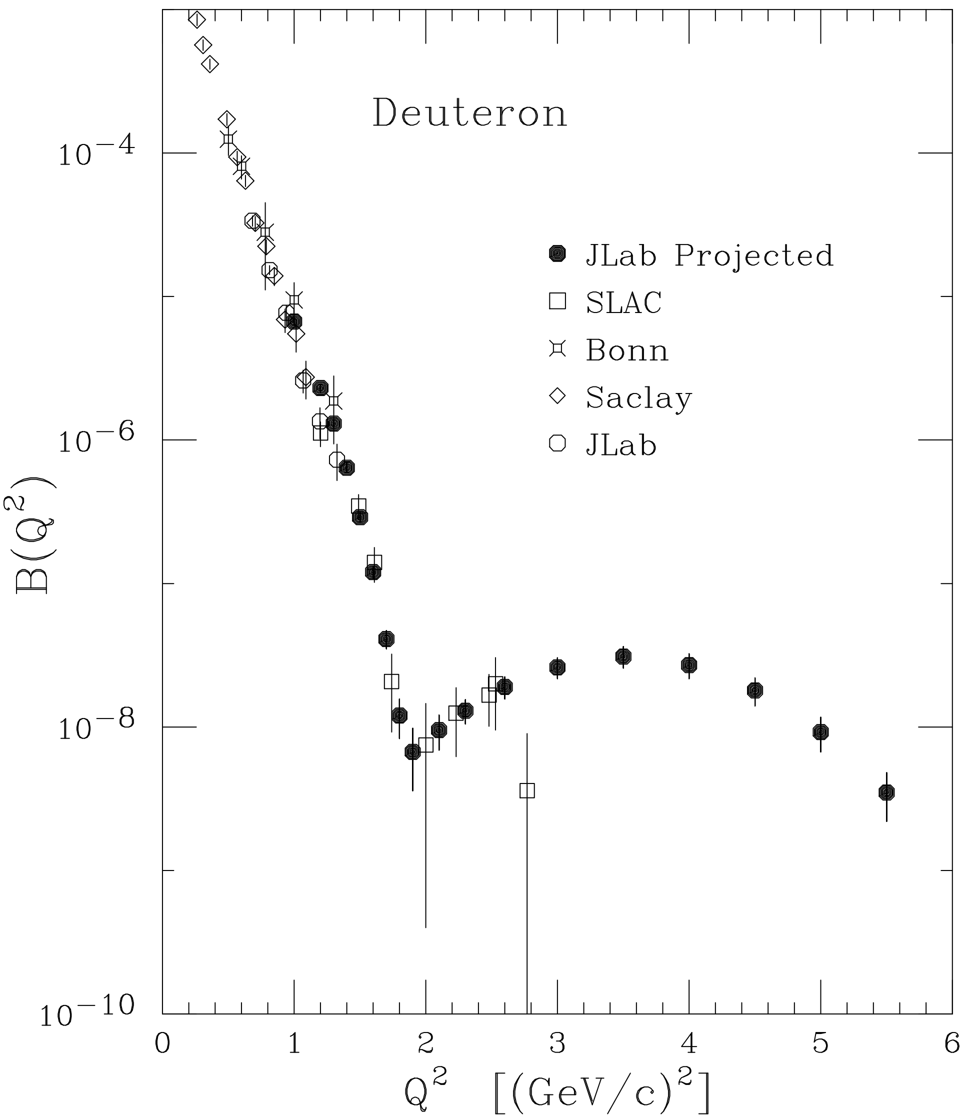

Figure 17: Projected deuteron magnetic form factor $B(Q^2)$ data from the proposed experiment. Also shown are recent JLab data [33] and older data from Bonn, Saclay and SLAC [7].

The estimated time required to measure $B(Q^2)$ to the maximum Q^2 possible and to map accurately its diffraction minimum is 40 days. An additional 4 days will be required for running with an empty replica target (with thicker end-caps) and 3 days for elastic electron-proton scattering at the same beam energies of the deuteron scattering. Proton scattering will be instrumental in understanding and periodically checking the performance of the double-arm spectrometer system.

Although the proposed spectrometer system can measure double-arm elastic electron-proton scattering only up to $Q^2 = 3.3$ (GeV$/c)^2$, the electron spectrometer has the capability to measure single-arm elastic electron-proton scattering up to the maximum beam energy available at the time of the experiment. The presently available maximum beam energy of 6 GeV would result in a direct measurement of the proton magnetic form factor G_M^p at $Q^2 = 10.5$ (GeV$/c)^2$. These measurements will be free of any experimental deficiencies that plague Rosenbluth separations and can provide pure G_M^p data with total errors of approximately 1.0% (similar to the SLAC NE11 errors [64]) in a very timely fashion.

We propose to perform this set of elastic proton measurements in addition to the ones required for the calibration and monitoring of the double-arm spectrometer system. The kinematics and all relevant parameters of the run plan for these extra measurements are given in Table 3. The projected G_M^p data from these measurements are shown in Figure 18 along with existing Stanford, SLAC, DESY and Bonn Rosenbluth separation data and direct $\theta = 180°$ elastic proton data from SLAC experiment NE4 [7, 65]. The Rosenbluth separation data are from extractions using only measurements from single elastic electron-proton scattering experiments, as compiled, with radiative correction improvements, in Ref. [66]. Shown also in the Figure is the fit by Bosted [67] of the G_M^p values from the "global" analysis of all proton elastic data by Walker *et al.* [68], and a new fit by Brash *et al.* [66] on G_M^p values extracted from selected elastic cross section data and the new JLab Hall A data [69] on the electric to magnetic proton form factor ratio G_E^p/G_M^p. It is evident from Figure 18 that the proposed measurements will be able to discriminate between the two fits and provide valuable input in understanding the extraction of the proton form factors from polarized and unpolarized measurements [66, 70] and in establishing firm values for the magnetic form factor.

The total amount of beam time required for the additional proton measurements is just 3 days including empty replica target running, making the total amount of requested beam time 50 days. An additional amount of beam time will be required for checking out and debugging the double-arm spectrometer system. Based on the SLAC NE4 experience (NE4 was awarded ~25 days of check-out time), a minimum of 15 days with a functional cryotarget will be needed for this purpose.

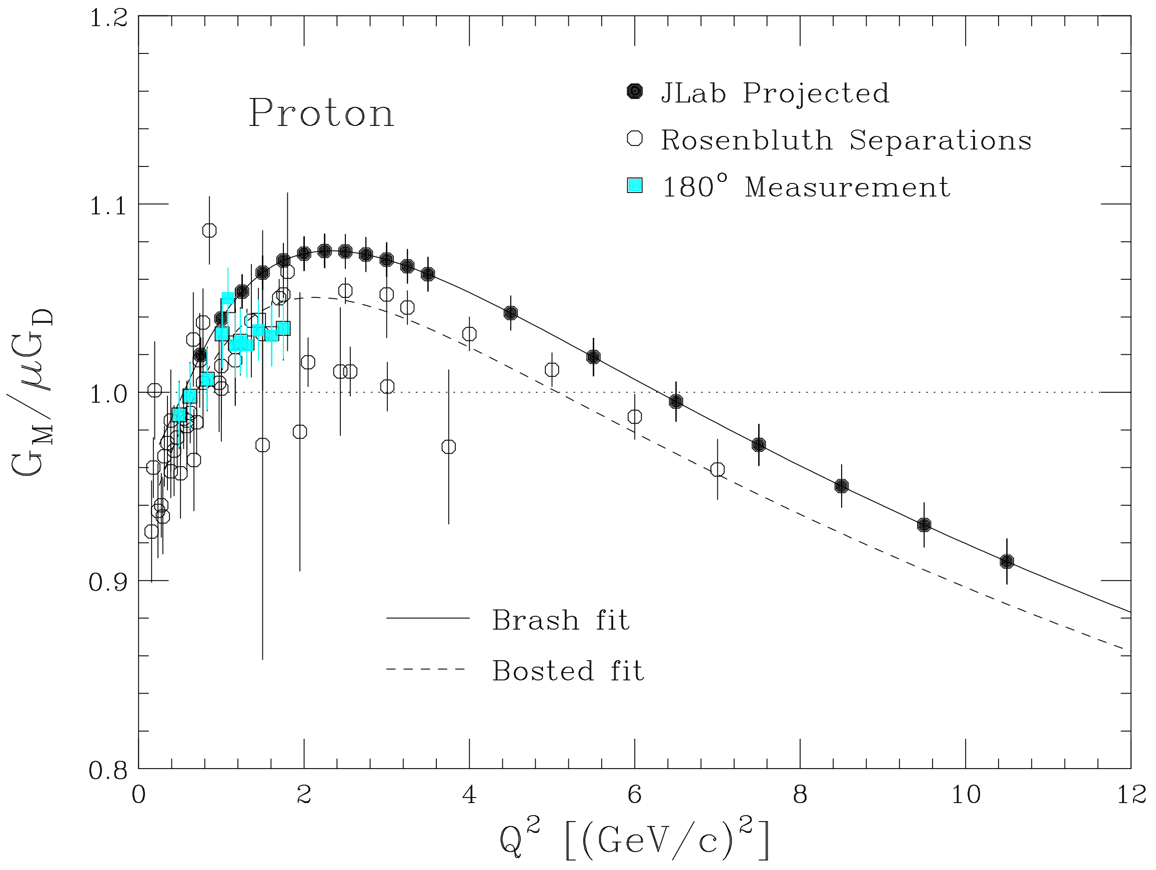

Figure 18: The proton magnetic form factor divided by the proton magnetic moment μ and the dipole formula $G_D = (1 + Q^2/0.71)^{-2}$. The open circles are Rosenbluth separation data from individual extractions using only measurements from single SLAC, Bonn, DESY and Stanford experiments, as compiled in Ref. [66]. The squares are the direct $\theta = 180°$ SLAC NE4 data [7, 65]. The curves are fits by Brash *et al.* [66] and Bosted [67] (see text). The solid circles are projected possible data from the proposed experiment.

7 Summary–Request

We propose to perform a precision measurement of the deuteron magnetic form factor over its diffraction minimum and up to the largest possible Q^2 limited by cross section sensitivity of one elastic event per day. The experiment can be performed in the Hall A Facility of JLab using a 180° magnetic spectrometer, built from existing magnets at JLab and surplus magnets readily available from other National Labs, to detect back-scattered electrons, and a $0°$ magnetic spectrometer, based on the hadron HRS, to detect forward-recoiling deuterons in coincidence with the electrons.

The proposed deuteron measurements will be of significant importance for the advancement of few-body nuclear physics and will provide data on a fundamental observable of the deuteron. The results of the experiment are expected to lead to the establishment of a consistent canonical hadronic model describing the electromagnetic structure of the deuteron. Additional possible measurements of the proton magnetic form factor will provide a precision set of data, free of Rosenbluth separation experimental deficiencies, and highly complementary to previous JLab data sets on the electric form factor.

We request the resources to design, build and calibrate the $180°/0°$ spectrometer system and the associated beam transport system, and a liquid deuterium/hydrogen target system with short cells and scattering chamber diameter. The required beam time is 50 days of data taking at 100% efficiency including empty target running and hydrogen calibrations. An additional minimum of 15 days of beam will be necessary for the check-out of the spectrometers and the detectors with a functional cryotarget.

ELECTRON-DEUTERON ELASTIC KINEMATICS

Q^2 $\left[(\mathrm{GeV}/c)^2\right]$	E (GeV)	E' (GeV)	P_d (GeV/c)	$d\Omega_e/d\Omega_d$
1.0	0.651	0.384	1.035	7.25
1.2	0.731	0.411	1.141	7.72
1.3	0.769	0.423	1.192	7.95
1.4	0.807	0.434	1.241	8.18
1.5	0.844	0.444	1.288	8.40
1.6	0.881	0.454	1.335	8.64
1.7	0.917	0.464	1.380	8.87
1.8	0.952	0.473	1.425	9.09
1.9	0.988	0.481	1.469	9.32
2.1	1.057	0.497	1.554	9.78
2.3	1.124	0.511	1.636	10.2
2.6	1.224	0.531	1.755	10.9
3.0	1.354	0.554	1.908	11.9
3.5	1.512	0.579	2.090	13.0
4.0	1.666	0.600	2.266	14.3
4.5	1.818	0.619	2.437	15.6
5.0	1.968	0.635	2.603	16.7
5.5	2.116	0.650	2.766	18.1
6.0	2.262	0.663	2.925	19.5

Table 1: Elastic electron-deuteron kinematics in the Q^2 range from 1.0 to 6.0 $(\mathrm{GeV}/c)^2$. The electron scattering angle is 180°. E is the incident beam energy, E' is the scattered electron energy, P_d is the recoil deuteron momentum. The last column is the Jacobian transformation of the solid angle for recoil detection.

B(Q^2) RUN PLAN SCENARIO

Q^2 $\left[(\mathrm{GeV}/c)^2\right]$	$B(Q^2)$	Cross Section (cm^2/sr)	Time (hr)	Counts	$\Delta B(Q^2)$ ($\pm$%)
1.0	6.7×10^{-6}	5.1×10^{-38}	3	3380	5
1.2	2.3×10^{-6}	1.4×10^{-38}	4	1280	6
1.3	1.3×10^{-6}	6.8×10^{-39}	6	980	6
1.4	6.4×10^{-7}	3.2×10^{-39}	8	640	7
1.5	2.9×10^{-7}	1.4×10^{-39}	14	520	8
1.6	1.2×10^{-7}	6.2×10^{-40}	24	390	10
1.7	4.1×10^{-8}	2.7×10^{-40}	48	350	15
1.8	1.2×10^{-8}	1.3×10^{-40}	72	260	30
1.9	6.7×10^{-9}	8.5×10^{-41}	72	175	46
2.1	9.5×10^{-9}	5.4×10^{-41}	72	120	27
2.3	1.3×10^{-8}	4.1×10^{-41}	72	90	19
2.6	1.9×10^{-8}	3.4×10^{-41}	48	50	17
3.0	2.6×10^{-8}	3.2×10^{-41}	48	47	17
3.5	3.1×10^{-8}	2.7×10^{-41}	48	40	17
4.0	2.7×10^{-8}	1.9×10^{-41}	48	27	20
4.5	1.8×10^{-8}	9.8×10^{-42}	72	22	23
5.0	9.2×10^{-9}	4.0×10^{-42}	120	15	27
5.5	3.5×10^{-9}	1.3×10^{-42}	192	8	38
Sub-Total			971		
Total			1056		

Table 2: Run plan scenario with cross section and counting rate estimates for the $B(Q^2)$ measurements. The rate estimates assume a 10 cm long liquid deuterium target, a beam current of 150 μA, an electron(recoil) spectrometer solid angle of 30(4) msr and a radiative correction factor of 0.7. The total time includes empty target running.

$\mathbf{G_M^p}$ SINGLE-ARM RUN PLAN

Q^2 $\left[(\mathrm{GeV}/c)^2\right]$	E (GeV)	E' (GeV)	Cross Section (cm^2/sr)	Time (hr)	Counts
3.5	2.253	0.388	2.4×10^{-36}	1	59700
4.5	2.800	0.402	6.7×10^{-37}	1	16950
5.5	3.342	0.411	2.3×10^{-37}	1	5900
6.5	3.882	0.419	9.4×10^{-38}	2	4760
7.5	4.421	0.424	4.2×10^{-38}	4	4280
8.5	4.958	0.429	2.1×10^{-38}	8	4200
9.5	5.495	0.432	1.1×10^{-38}	15	4150
10.5	6.030	0.435	6.1×10^{-39}	26	4000
Sub-Total				58	
Total				72	

Table 3: Kinematics, cross section and counting rate for the proposed measurements of the proton magnetic form factor G_M^p. The rate estimates assume a 10 cm long liquid hydrogen target, a beam current of 150 μA, an electron spectrometer solid angle of 30 msr and a radiative correction factor of 0.7. The total time includes empty target running.

References

[1] J. Carlson and R. Schiavilla, Rev. Mod. Phys. **70**, 743 (1998).

[2] M. Garçon and J.W. Van Orden, Advances in Nucl. Phys. **26**, 293 (2001).

[3] R. Gilman and F. Gross, J. Phys. **G28**, R37 (2002).

[4] I. Sick, Prog. Part. Nucl. Phys. **47**, 245 (2001).

[5] C.E. Carlson, J.R. Hiller and R.J. Holt, Annu. Rev. Nucl. Part. Sci. **47**, 395 (1997).

[6] L.C. Alexa *et al.*, Phys. Rev. Lett. **82**, 1374 (1999); and references therein.

[7] P.E. Bosted *et al.*, Phys. Rev. **C42**, 38 (1990); and references therein.

[8] T.W. Donnelly and A.S. Raskin, Annals Phys. **169**, 247 (1986).

[9] J. Arvieux and J.M. Cameron, Advances in Nucl. Phys. **18**, 107 (1987).

[10] M. Bouwhuis *et al.*, Phys. Rev. Lett. **82**, 3755 (1999); and references therein.

[11] D. Abbott *et al.*, Phys. Rev. Lett. **84**, 5053 (2000); and references therein.

[12] E.L. Lomon, Annals Phys. **125**, 309 (1980); and references therein.

[13] T.W. Donnelly and I. Sick, Rev. Mod. Phys. **56**, 461 (1984).

[14] R. Dymarz and F.C. Khanna, Nucl. Phys. **A516**, 549 (1990).

[15] A. Amghar, N. Aissat and B. Desplanques, Eur. Phys. J. **A1**, 85 (1998).

[16] B.D. Keister and W.N. Polyzou, Advances in Nucl. Phys. **20**, 225 (1991).

[17] J. Carbonell, V.A. Karmanov and J.F. Mathiot, Phys. Rep. **300**, 215 (1998).

[18] F. Gross, in *Modern Topics in Electron Scattering*, ed. B. Frois and I. Sick (World Scientific, Singapore, 1991).

[19] E. Salpeter and H. Bethe, Phys. Rev. **84**, 1232 (1951).

[20] J.W. Van Orden, N. Devine and F. Gross, Phys. Rev. Lett. **75**, 4369 (1995).

[21] E. Hummel and J.A. Tjon, Phys. Rev. **C42**, 423 (1990).

[22] D.R. Phillips, S.J. Wallace and N.K. Devine, Phys. Rev. **C58**, 2261 (1998).

[23] F. Gross, arXiv:nucl-th/0212036, submitted to Few-Body Systems Suppl., December 2002.

[24] J.W. Van Orden, presented at the *Topical Workshop on the Deuteron*, Florida International University, Miami, Florida, March 2003.

[25] T-S. Cheng and L.S. Kisslinger, Phys. Rev. **C35**, 1432 (1987).

[26] W.P. Sitarski *et al.*, Phys. Rev. **C36**, 2479 (1987); P.G. Blunden *et al.*, Phys. Rev. **C40**, 1541 (1989).

[27] H. Dijk and B.L.G. Bakker, Nucl. Phys. **A494**, 438 (1989).

[28] S.J. Brodsky and G.R. Farrar, Phys. Rev. Lett. **31**, 1153 (1973).

[29] V.A. Matveev, R.M. Muradyan and A.N. Tavkhelidze, Lett. Nuovo Cimento **7**, 719 (1973).

[30] S.J. Brodsky, C-R. Ji and G.P. Lepage, Phys. Rev. Lett. **51**, 83 (1983).

[31] S.J. Brodsky and J.R. Hiller, Phys. Rev. **D46**, 2141 (1992).

[32] A. Kobushkin and A. Syamtomov, Phys. Rev. **D49**, 1637 (1994).

[33] K. McCormick *et al.*, in preparation for submission to Phys. Rev. **C**.

[34] D. Abbott *et al.*, Phys. Rev. Lett. **82**, 1379 (1999).

[35] A.T. Katramatou *et al.*, Nucl. Instrum. Meth. **A267**, 448 (1988).

[36] G.G. Petratos, SLAC Report NPAS-TN-86-7 (1986).

[37] D.M. Nikolenko *et al.*, Phys. Rev. Lett. **90**, 072501 (2003).

[38] R. Schiavilla and D.O. Riska, Phys. Rev. **43**, 437 (1991); R.B. Wiringa, V.G.J. Stoks and R. Schiavilla, Phys. Rev. **C51**, 38 (1995).

[39] F. Gross, Phys. Rev. **186**, 1448 (1969); Phys. Rev. **D10**, 223 (1974); Phys. Rev. **C26**, 2203 (1982); and references therein.

[40] R. Blankenbecler and R. Sugar, Phys. Rev. **142**, 1051 (1966); A.A. Logunov and A.N. Tavkhelidze, Nuovo Cimento **29**, 380 (1963).

[41] H. Ito and F. Gross, Phys. Rev. Lett. **71**, 2555 (1993).

[42] T.W. Allen, W.H. Klink and W.N. Polyzou, Phys. Rev. **C62**, 054002 (2000).

[43] F.M. Lev, E. Pace and G. Salmè, Phys. Rev. **C62**, 064004 (2000).

[44] R. Schiavilla and V.R. Pandharipande, Phys. Rev. **C65**, 064009 (2002).

[45] R.G. Arnold *et al.*, Phys. Rev. Lett. **35**, 776 (1975).

[46] S.J. Brodsky and B.T. Chertok, Phys. Rev. **D14**, 3003 (1976).

[47] N. Isgur and C.H. Llewellyn Smith, Phys. Rev. Lett. **52**, 1080 (1984); Phys. Lett. **B217**, 535 (1989).

[48] G.R. Farrar, K. Huleihel and H. Zhang, Phys. Rev. Lett. **74**, 650 (1995).

[49] E.C. Schulte *et al.*, Phys. Rev. Lett. **87**, 102302 (2001); and references therein.

[50] L.E. Marcucci, D.O. Risca and R. Schiavilla, Phys. Rev. **C58**, 3069 (1998).

[51] P.L. Chung *et al.*, Phys. Rev. **C37**, 2000 (1988).

[52] J. Carbonnel and V.A. Karmanov, Eur. Phys. J. **A6**, 9 (1999).

[53] H. Arenhövel, F. Ritz and T. Wilbois, Phys. Rev. **C61**, 034002 (2000).

[54] R. Cramer *et al.*, Z. Phys. **C29**, 513 (1985).

[55] S. Platckov *et al.*, Nucl. Phys. **A510**, 740 (1990).

[56] *Nuclei, Nucleons, Quarks – Nuclear Science in the 1990's*, Long Range Plan by the DOE/NSF Nuclear Science Advisory Committee, December 1989.

[57] *Opportunities for Nuclear Science – A Long Range Plan for the Next Decade*, by the DOE/NSF Nuclear Science Advisory Committee, April 2002.

[58] G.G. Petratos, *High-Q^2 Few-Body Form Factors*, presented at the 12 GeV JLab PAC18 meeting, July 2000.

[59] A.T. Katramatou, SLAC Report SLAC-NPAS-TN-86-08, 1986.

[60] G.G. Petratos *et al.*, *Measurement of the Electric and Magnetic Elastic Structure Functions of the Deuteron at Large Momentum transfers*, CEBAF Proposal E91-26, 1991.

[61] O. Hashimoto *et al.*, *Spectroscopic Study of Lambda Hypernuclei up to Medium-Heavy Mass Region through the $(e, e'K^+)$ Reaction*, JLab Proposal E01-011, 2001.

[62] *Conceptual Design Report, Basic Experimental Equipment*, CEBAF, April 1990.

[63] K.S. Kumar *et al.*, *A Precision Measurement of the Weak Mixing Angle in Møller Scattering*, SLAC Proposal E158, 1997.

[64] L. Andivahis *et al.*, Phys. Rev. **D50**, 5491 (1994).

[65] A.T. Katramatou and G.G. Petratos, private communication.

[66] E.J. Brash *et al.*, Phys. Rev. **C65**, 051001 (2002).

[67] P.E. Bosted, Phys. Rev. **C51**, 409 (1995).

[68] R.C. Walker *et al.*, Phys. Rev. **D49**, 5671 (1994).

[69] M.K. Jones *et al.*, Phys. Rev. Lett. **84**, 1398 (2000); O. Gayou *et al.*, Phys. Rev. Lett. **88**, 092301 (2002).

[70] J. Arrington, arXiv:hep-ph/0209243, submitted to Eur. Phys. J., September 2002.